EXPERIMENTAL EVALUATION OF HEAT TRANSFER CHARACTERISTICS OF SILICA NANOFLUID

By

Zihao Zhang

SUBMITTED TO THE DEPARTMENT OF MECHANICAL ENGINEERING IN PARTIAL FULFILLMENT OF THE REQUIREMENTS FOR THE DEGREE OF

BACHELOR OF SCIENCE IN MECHANICAL ENGINEERING

AT THE

MASSACHUSETTS INSTITUTE OF TECHNOLOGY

JUNE 2010

Signature of Author: _____

Department of Mechanical Engineering
May 10, 2010

Certified by: _____

Lin-Wen Hu
Associate Director of MIT Nuclear Reactor Laboratory
Thesis Supervisor

Accepted by: _____

John H. Lienhard V
Professor of Mechanical Engineering
Chairman of Undergraduate Thesis Committee

EXPERIMENTAL EVALUATION OF HEAT TRANSFER CHARACTERISTICS OF SILICA NANOFLUID

By

Zihao Zhang

Submitted to the Department of Mechanical Engineering on May 10, 2010 in the partial fulfillment of the requirements for the Degree of Bachelor of Science in Mechanical Engineering

ABSTRACT

The laminar convective heat transfer characteristics were investigated for silica nanofluid. An experimental loop was built to obtain heat transfer coefficients for single-phase nanofluids in a circular conduit in laminar flow regime. Thermal conductivity and viscosity measurements were conducted on the silica nanofluid to determine the thermophysical properties needed for analysis. Qualitative tests showed that the silica nanofluid was a stable colloidal suspension under the temperature range expected in the heated flow loop up to 80°C. Experiments were performed in the flow loop for the silica nanofluid at 0.2 Vol.%, 1 Vol.%, and 5 Vol.% concentrations. It was found that the heat transfer coefficient increased only slightly, but the heat transfer increase is within the experimental uncertainty of ±10%. The experiment results were in agreement with correlations using the as-measured thermal conductivity and viscosity of the nanofluid. It is concluded that silica nanofluid tested in this study showed no abnormal heat transfer enhancement in the laminar flow regime.

Thesis Supervisor: Lin-Wen Hu
Title: Associate Director of MIT Nuclear Reactor Laboratory

ACKNOWLEDGEMENTS

The author has been an undergraduate student at MIT from Fall 2006 until Spring 2010. He entered the Department of Mechanical Engineering in Fall 2007. Previously, he has worked on an undergraduate research project with Professor Martin Culpepper developing medical equipment. This has led to a patent publication. In the Fall 2010, the author will continue his passion in mechanical engineering as a Ph.D. candidate at the Georgia Institute of Technology.

I would like to thank my thesis supervisor Dr. Lin-Wen Hu for advising me of the guidelines and content necessary for my thesis to come together. She has been very patient with me throughout this endeavor, and we have faced challenges together in stride. I would like to thank Dr. Thomas McKrell for helping me solve the problems going on in the Green Lab. He was been extremely instrumental in showing me the ways of the lab and getting parts and pieces come together. Also, I give a special thanks to Bao Truong, because he helped me become acquainted to the experiment. He has been the extra set of hands I desperately need to get the project done.

In my personal life, I'd like to thank my family and parents, Ming and Manfang. They were always there whenever I needed personal guidance as well as some technical guidance (Ming is a Ph.D. graduate in Physics from MIT in 1991).

TABLE OF CONTENTS **PAGE #**

LIST OF FIGURES

LIST OF TABLES

LIST OF SYMBOLS

Symbol	Definition
A	Flow cross-section area
c^*	Nanofluid specific heat
c_{pp}	Nanoparticle specific heat
c_w	Base fluid specific heat
D_i	Inner diameter
D_o	Outer diameter
h	Heat transfer coefficient
k	Thermal conductivity (general)
k^*	Nanofluid thermal conductivity
L	Total section length
L_e	Entry length
$\dot{m}$	Flow rate
μ	Fluid viscosity (general)
μ_{nf}	Nanofluid viscosity
μ_w	Water viscosity
Nu	Nusselt Number
P	Pressure
ϕ	Percent volume concentration
Pr	Prandtl Number
Q	Power
q	Heat flux
r	Radius
σ	Standard deviation
Re	Reynolds Number
ρ^*	Nanofluid density
ρ_p	Particle density
ρ_w	Base fluid density
T_B	Bulk temperature
T_w	Wall temperature
V	Average velocity
w	Percent weight concentration
x	Length in section
x_+	Dimensionless distance

CHAPTER 1. THESIS OBJECTIVE

The objective of this thesis is to measure the convective heat transfer properties of silica nanofluid in laminar flow regime. A flow loop was modified to obtain the heat transfer coefficients of the experimental fluid at different temperatures and Reynolds numbers. The nanofluid of interest is silica (SiO_2) nanoparticle dispersion in water. Data collected on temperatures of the heated test section were used to calculate the heat transfer coefficients at various axial positions. The primary questions assessed for this research project are: Does silica nanofluid have significant advantage in thermal conductivity over the base fluid water? Does the nanofluid remain stable at elevated temperatures? Also, does the nanofluid offer enhanced heat transfer properties beyond theory prediction? The results from this experiment will provide answers to these questions. Finally, a conclusion is made that addresses whether the silica nanofluid enhances heat transfer in laminar flow regime.

CHAPTER 2. INTRODUCTION

Section 2.1. BACKGROUND IN HEAT TRANSFER

Heat transfer engineering is the study of energy transport and exchange between kinetic mediums. Important parameters related to heat transfer are flow rate, flow pattern or geometry, fluid thermal physical properties, temperature, pressure, and more. The thermal conductivity is important for understanding the temperature dependence to isotropic energy transfer. Using the heat conduction relation, the thermal conductivity (k) is defined as the rate of heat flow (dQ/dt) per unit area in a temperature gradient,

$$\frac{dQ}{dt}\frac{1}{A} = -k\frac{dT}{dx}. \tag{1}$$

This proposes that thermal conductivity values can affect temperature profiles of flows that are supplied with power. Thus, the thermal conductivity, k, is crucial in determining heat transfer characteristics. The mass flow characteristics have an important role in heat transfer as well. Observing the first law of thermodynamics work equation,

$$\dot{m} = \frac{1}{c_p}\frac{dQ}{dT}. \tag{2}$$

It is seen that the mass flow ($\dot{m}$) relates the total internal energy to the temperature, linearly proportional to c_p, which represents the specific heat of the mass. The specific heat is a unit that determines the increase of energy for a differential increase in temperature of a mass. The fluid dynamic behavior of the mass flow is discussed in a later section.

Section 2.2. RECENT WORKS IN NANOFLUID CONVECTIVE HEAT TRANSFER RESEARCH

Recent works have been published on similar interests and experiments. These research findings have explored thermophysical properties of nanofluids and their theoretical enhancement toward heat transfer. Models and correlations have been developed to generalize the behavior of these nanofluids under varying conditions. Other findings have emphasized different flow regimes and how they can affect heat transfer. These studies have all emphasized the heat transfer enhancement of different nanofluids.

Two papers that were published by former students at MIT are the basis for this study. The first, published by Rea Ref. [16], used alumina and zirconia nanofluids in an experimental study of heat transfer characteristics in laminar flow. In addition, this study also produced results on viscous pressure drop of nanofluids. The study found that the nanofluids display slight increase in heat transfer coefficient over water, but increased pressure loss due to the higher viscosity of the nanofluids. Since the study was produced under laminar flow conditions, the heat transfer in the entry region was taken into account.

The other study, written by Williams Ref. [19] a former graduate student at MIT, conducted tests of the same nanofluids but subjected them to another flow loop that was designed for higher flow rates for turbulent flow study (9000<Re<63000). Under turbulent flow, the heat transfer coefficient correlation was modeled with the Dittus-Boelter relation. Williams concluded that nanofluids have no abnormal improvement on convective heat transfer in turbulent regimes beyond that predicted by theory if nanofluid properties were used .

A study developed by several Chinese researchers and the University of Leeds (Ding et. al.) Ref. [8] have investigated how different of methods of convective heat transfer affects the heat transfer coefficient enhancement. By comparing natural versus forced convective heat transfer, they estimated that heat transfer was best at the entry region of the forced fluid in a circular pipe. In agreement with Williams, the heat transfer behavior is primarily determined by the viscosity and conductivity of the nanofluid.

A paper summarized an International Benchmark Exercise of nanofluid property measurements details the behavior of different nanofluids [2]. The study involved capturing TEM images of nanofluids, showing the size and geometry of nanoparticles. The study provided extensive results on thermal conductivity measured primarily by thermal hot wire techniques. The study concluded no abnormal enhancement was observed in the nanofluids tested, beyond the prediction of the classical mixed medium theory.

Silica nanofluid is discussed in another study published by the University of Alaska, Fairbanks (Das) Ref. [6] Their study consisted nanoparticles suspended in 60%/40% ethylene glycol and water, respectively. They determined the thermophysical properties of the nanofluid by conducting quantitative tests of the nanofluid at varying concentrations. Their correlation is given in respect to the turbulent Dittus-Boelter or Gnielinski Nusselt number correlations of water. Reynolds numbers for these correlations range from 3000 to 1E6. The group acquired several solutions of silica nanofluid of differing particle sizes of 20, 50 and 100 nm. However, the particle size was found to not affect the overall Nusselt correlation.

CHAPTER 3. HEAT TRANSFER IN LAMINAR FLOW REGIME

Section 3.1. FLOW PARAMETERS

3.1.1. Liquid Properties

A fluid consists of molecules that are characterized by its collective rheological and thermophysical properties. Water, the base fluid used in this study, exists in three phases: solid, liquid, and gaseous. A fluid under different phases possesses different behavior. To determine the thermophysical behaviors of the fluid, steam tables are compiled for calculation of energy gain/loss, entropy, heat flux, etc. Examining the steam tables for water Ref. [10], it is shown that thermal transport is significantly affected by phase.

In liquid phase, thermodynamic equations are determined by the fluid density, specific heat, viscosity and conductivity. The Prandtl number is a dimensionless number that describes the viscosity, conductivity and specific heat ($\mathrm{Pr} = \frac{\mu c_p}{k}$) of the fluid. Under liquid phase and atmospheric pressure conditions, the values for these parameters are significantly different from those under the gaseous phase. Table 3.1 shows the difference between these parameters of water at 100°C.

Table 3.1. Thermophysical properties of water at 100°C

Properties, [10]	Liquid Phase	Gaseous Phase
Density (ρ_w)	958.35 [kg/m^3]	0.59817 [kg/m^3]
Specific heat (c_w)	4215.7 [J/kg K]	2080.0 [J/kg K]
Viscosity (μ_w)	2.8174E-4 [Pa s]	1.2269E-5 [Pa s]
Conductivity (k_w)	0.67909 [W/m K]	0.02510 [W/m K]

With these property changes kept in mind, it is essential to design an experiment that is kept in single phase. The phase change within a tested section could mean heat transfer properties that cannot be easily modeled. Figure 3.1 shows how convective boiling produces regions of complex behavior Ref. [9]. The vapor phase involves small bubbles formed at nucleation sites, and as they coalesce, could form larger bubbles. Since the focus

of this study is single-phase laminar flow, the heat flux and fluid temperature were controlled to maintain single-phase liquid throughout the heated test section.

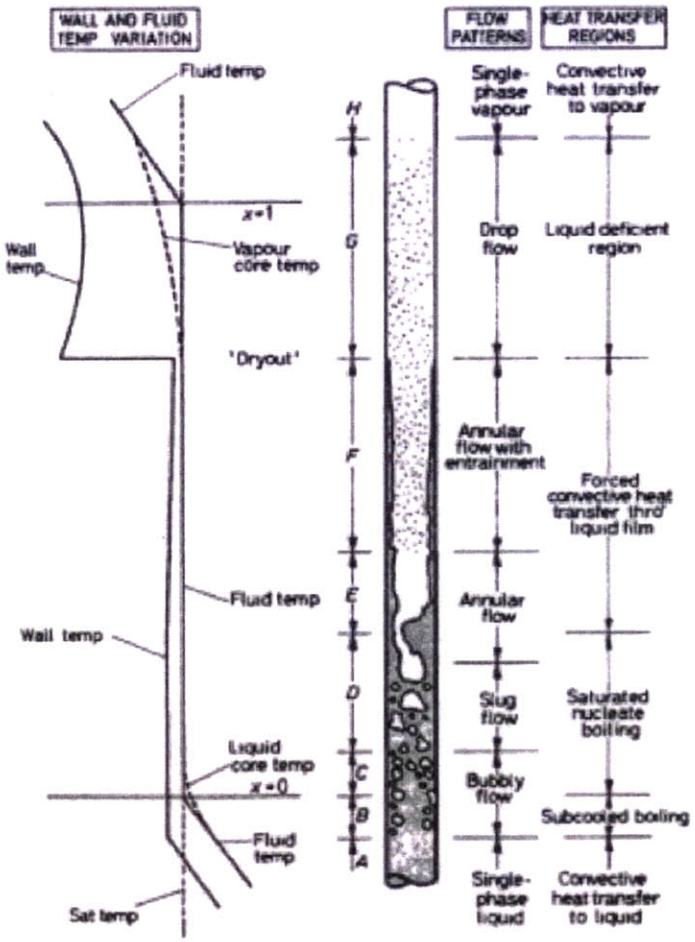

Figure 3.1. Two-phase steam bubble development in vertical tube. [9].

3.1.2. Laminar Flow Regime

The flow regime can be determined by the Reynolds number, given as,

$$\mathrm{Re} = \frac{\rho V D_i}{\mu}. \tag{3}$$

The Reynolds number calculates the average velocity of the flow (V), and fluid properties density (ρ) and fluid viscosity (μ). In the circular conduit of diameter D_i, the Reynolds number determines how the fluid travels along the wall of the pipe versus the center or

bulk area. This boundary layer at the wall can be important for thermodynamic calculations, as the flow here can affect the conduction of heat through the fluid. Applying the Navier-Stokes equation Ref. [3], the fully developed flow profile can be given as,

$$V_z(r) = -\frac{D_i^2}{16\mu}\left(\frac{\partial P}{\partial z}\right)\left[1-\left(\frac{2r}{D_i}\right)^2\right]. \tag{4}$$

This equation indicates that the laminar flow should have a parabolic flow profile varying with distance from the center of flow (r) for a constant viscosity and steady pressure loss along the length of the pipe flow (x),

$$\Delta P = \frac{64}{\mathrm{Re}}\left(\frac{x}{D_i}\right)\left(\frac{\rho V^2}{2}\right). \tag{5}$$

An illustration of this type of flow is shown in Figure 3.2.

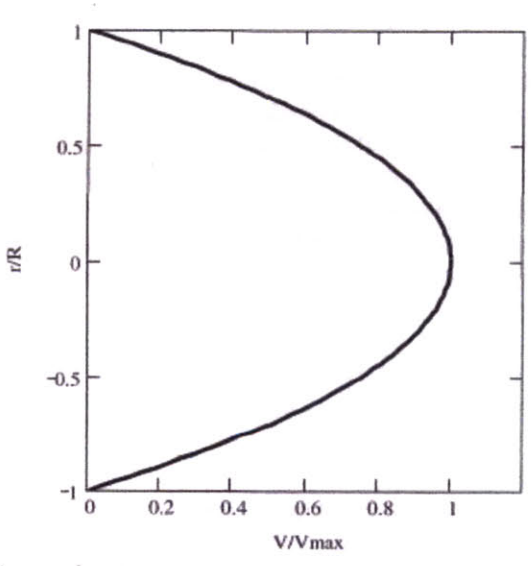

Figure 3.2. Parabolic fully-developed laminar flow in pipe of constant pressure loss [3].

For a pressure loss that is not constant and not fully developed, the flow profile is more complex. This occurs when the fluid is in the entry region of the circular conduit. The laminar entry length (L_e) was determined with best-fit approximation Ref. [18],

$$\frac{L_e}{D_i} = \frac{0.60}{0.035\mathrm{Re}+1} + 0.056\mathrm{Re}. \quad (6)$$

When developing the experimental apparatus, it is important to design the equipment (i.e. pump) and dimensions (i.e. heated test section) according to these parameters in laminar flow.

3.1.3. Laminar Flow Heat Transfer Characteristics

By applying the fundamental first law of thermodynamics, the temperature and heat transfer characteristics can be determined. Because of the non-constant flow profile of the transport flow, the thermal characteristics are determined with bulk or average flow. An important parameter is mass flow rate,

$$\dot{m} = \rho V A. \quad (7)$$

The fluid behavior is generalized in the entire cross-sectional area of the circular conduit ($A = \pi \frac{D_i^2}{4}$). The above equation can then be applied to the first law of thermodynamics (Eq. 2). This gives the rate of temperature change that is proportional to the energy input into the system. This is meaningful because the ideal heated test section applies a constant heat flux where,

$$q = \frac{dQ}{\pi D_i dx}. \quad (8)$$

The heat transfer coefficient is defined as a ratio of heat flux to the temperature difference between bulk fluid and heat transfer surface. The heat transfer coefficient h is defined as,

$$h = \frac{q}{T_R - T_b}. \quad (9)$$

It takes into account in a fully developed laminar flow of the temperature difference between the inner wetted surface (T_R) of the circular conduit and the bulk temperature flow (T_b). Assuming the heat flux is constant, the heat transfer coefficient should scale

inversely to the temperature difference. The inner wall temperature can be determined from the outer wall temperature using the conduction equation from the Williams study Ref. [19],

$$T_{wi} = T_{wo} - \frac{Q}{2\pi k_S L}\left[\frac{D_o^2}{D_o^2 - D_i^2}\log\left(\frac{D_o}{D_i}\right) - 0.5\right]. \tag{10}$$

*k_S is determined by the thermal conductivity of the pipe wall. For stainless steel heated test section, $k_S = 0.0127T_w + 13.23188$.

The heat transfer characteristic is typically compared using the dimensionless Nusselt number, $Nu = \frac{hL}{k}$, which is the ratio between the convective to conductive heat transfer. When the flow becomes fully developed in a circular pipe, the Nusselt number becomes constant, Nu = 4.364 Ref. [11].

Section 3.2. WATER AND NANOFLUID PROPERTIES

3.2.1. Literature and Data

In the study of thermodynamics, steam tables are normally used as source of reference for vapor and liquid-phase properties of water. The main properties adopted for this study from the steam tables are density, viscosity, specific heat, and thermal conductivity. Since these properties varies with temperature, it is important to use the temperature-dependent properties in the analysis because the fluid temperature in the heated section of the experimental loop varies with axial location, heat flux, and flow rate.

3.2.2. Curve-Fitting of Temperature Dependent Water Properties

The property data for saturated water fluid density, viscosity, conductivity, and Prandtl number were obtained from steam properties tables Ref. [10]. The temperature data points range between 10^{o}C to 100^{o}C at intervals of 5^{o}C. All values are accurate to five significant digits.

The property data are approximated as fourth order polynomials. The Matlab function "polyfit" was used to obtain the curve fits. The "plot" function is used to compare the empirical property data points to the polynomial model, varying with the same temperature range from the property tables. The comparisons are shown below in Table 3.2.

Table 3.2. Fourth-order polynomial curve fits of water properties from steam table

Water Properties (F)	A	B	C	D	E
Density (ρ_w) [kg/m^3]	-9.8329E-8	3.4295E-5	-6.9601E-3	3.5056E-2	9.9998E+2
Viscosity (μ_w) [kg/s m]	2.1033E-11	-63829E-9	7.7138E-7	-4.8578E-5	1.7179E-3
Conductivity (k_w) [W/K m]	5.0132E-10	-1.0157E-7	-3.0626E-6	2.0111E-3	5.6022E-1
Prandtl number (Pr)	1.8571E-7	-5.5900E-5	6.6321E-3	-4.0026E-1	1.2806E+1
$F(T) = A \cdot T^4 + B \cdot T^3 + C \cdot T^2 + D \cdot T + E$					

Section. 3.3. FLUID PROPERTY TESTS

For the purpose of measuring the thermophysical properties of the nanofluid of interest, verification tests are conducted using a thermal conductivity probe and viscometer with known properties on pure fluids. Two fluids, de-ionized water and propylene glycol, are used because they demonstrate different qualities while still both safe to handle. Propylene glycol is fully miscible with water and acetone, making it easy to clean off surfaces of test apparatuses.

3.3.1. KD2 Pro thermal conductivity measurements

The equipment used to test fluid thermal conductivity is the Decagon KD2 Pro sensor (Figure 3.3). The probe uses the transient line heat source method Ref. [7]. A measurement cycle consists of 15-minute temperature equilibration time and a 60-second measurement time. The probe measures fluid temperature at a rate of 1 reading per second. The data measurement has a ±5% error.

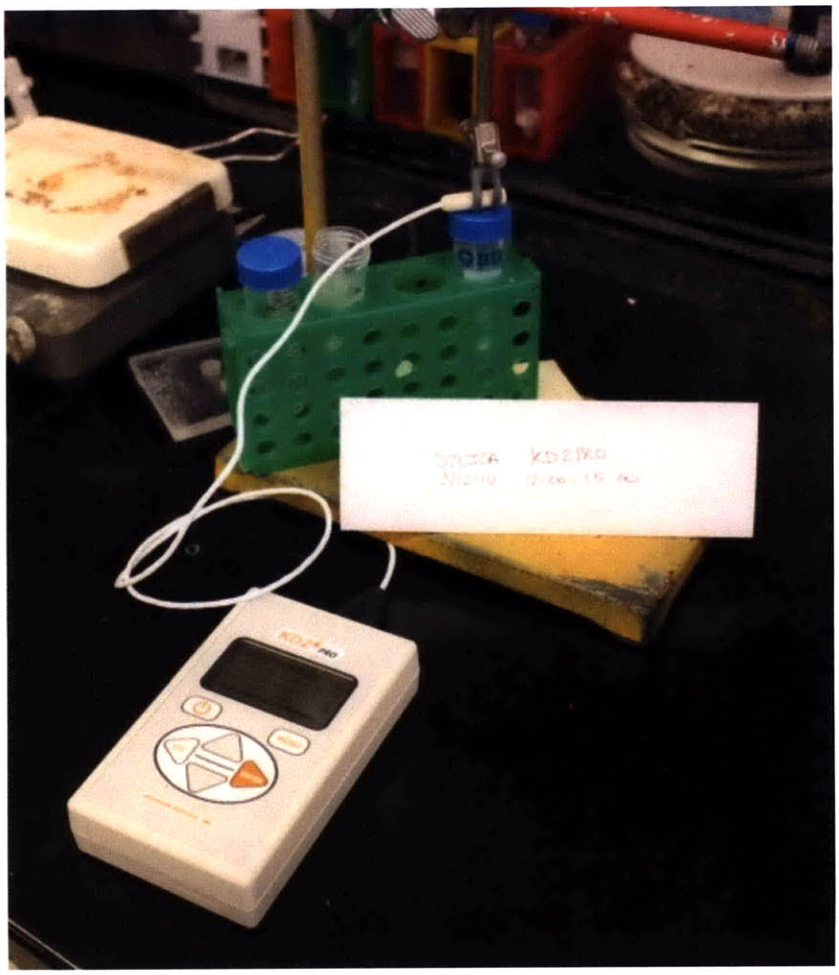

Figure 3.3. KD2 Pro thermal conductivity measurement setup.

Factors that may cause measurement errors in the KD2 Pro probe include fluid convection and vibrations, probe orientation, and temperature equilibrium between the probe and fluid. Since the fluid sample may not be in a constant temperature environment or situated in a water bath, the data accuracy remains ensured by a corrective linear drift term Ref. [7]. Thermal convection still occurs even in a seemingly still and homogeneous fluid sample. This can cause temperature gradients and can increase conduction readings from the probe. For ideal and highest accuracy, the sample and apparatus should be placed on a vibration reduction table. The probe orientation can also affect readings since bulk convective gradients generally rise vertically upward. Thus, the conduction probe makers recommend that a fixture is used to place the KD2 Pro probe vertically into the sample.

Most importantly, the thermal conductivity readings can be off when the probe and sample fluid do not reach temperature equilibrium before readings.

To ensure the best accuracy, the KD2 Pro probe was attached to a tablestand and oriented as vertically as possible. The fluid samples were put in 50mL Falcon test tubes. To allow for thermal equilibrium with the fluid, the probe was submerged into the fluid sample for more than 15 minutes before first measurement. Successive measurements were made every 15 minutes. The KD2 Pro sensor has settings to take measurements at certain time intervals. 10 measurements were made for each fluid sample.

With de-ionized water at around 25^{0}C, it is expected from steam tables that the thermal conductivity of water is 0.607 W/m ^{0}K. Using the fourth-order polynomial fit for analysis and comparison of Rea results, the measured thermal conductivity can be compared to the modeled value. Water gave ±3% error from measured readings. Average water thermal conductivity is k_{water} = 0.596 W/m ^{0}K with standard deviation of 0.012 W/m ^{0}K. Figure 3.4 shows the thermal conductivity measurements as well as expected values.

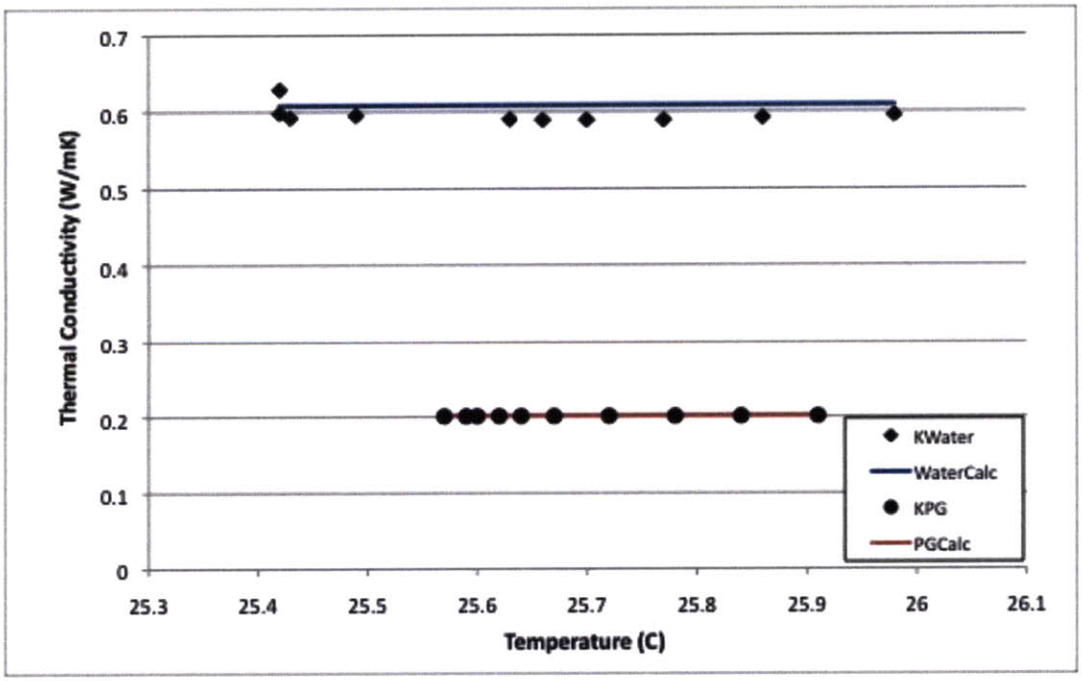

Figure 3.4. Plot showing the precision of KD2 Pro thermal heated probe.

While the thermophysical properties of water are in standard steam tables and have a fourth-order polynomial model, data on the thermal conductivity of propylene glycol has yet to be obtained Ref. [1] describes experiments conducted on propylene glycol. Using its results, a fourth-order polynomial model of thermal conductivity was established in terms of temperature from 24.64^{0}C to 80^{0}C. The curve fit was established at less than 0.2% error. Using similar procedures used to measure the thermal conductivity of water, and at similar fluid temperatures, the average thermal conductivity is k_{PG} = 0.201 W/m ^{0}K with standard deviation close to zero as the decimal values did not change in all data points. The error from the model is between 0.34% and 0.39%. Figure 3.4 shows the thermal conductivity results of propylene glycol in comparison with that of water.

3.3.2. Brookfield viscometer measurements

The nanofluid of interest is a mixed substance that consists of fine surfactant-coated nanoparticles. As these solids mix with water, the viscosity increases. Again, both de-ionized water and pure propylene glycol are used to demonstrate the operation of the viscometer. The equipment used to measure liquid viscosity is a Brookfield LVDV-II digital viscometer (Figure 3.5).

Figure 3.5. Brookfield digital viscometer with cone/plate spindle.

The viscometer uses a range of metal spindles to measure the shear forces in sample fluids. Mechanically, the shear forces cause the viscometer motor-driven spring to torque, which determines the calibrated viscosity values. The viscometer allows changes in rotational speed such that torque ranges can be attained for differing viscosities. Generally, low viscosity fluids require spindles with larger surface areas and at high rotational speeds. High viscosity is measured with smaller spindles and lower speeds. In addition, a water bath can be incorporated into the system to maintain constant temperatures for fluids with properties that are highly temperature dependent.

For the measurement of water and propylene glycol, the expected viscosity values are relatively low, within an order magnitude of 10^{-1} to 10^{2} centipoise (1 cP = 0.001 Pa*s). The spindle used to accurately measure these ranges is the cone/plate spindle. Using the constant temperature water bath, the fluid viscosity can be varied and compared against property table values. The measurement uncertainty within these ranges could be large because the viscometer reading has a possible error of ±1 cP from the maximum value of full viscosity (100 cP).

The measurement of water using the Brookfield viscometer produced results that are within the magnitude range of the property model. For water, the average viscosity is μ_w = 1.40 cP at 21.7°C measured at 100 rpm. According to the fourth-order polynomial fit model of water viscosity described in Table 3.2, the viscosity at similar temperature is at μ = 0.96 cP. Although the error of range is large, between 42% to 48%, the standard deviation is calculated at 0.017 cP. This means the viscometer is highly repeatable and can produce good results assuming correct spindle selection.

For propylene glycol, the spindle speeds are reduced significantly to 10 rpm in order to obtain a torque range that is readable by the motor-driven spring. The average viscosity is μ_{PG} = 52.2 cP at 21.9°C. With viscosity data obtained from Ref. [5], a model is developed to estimate propylene glycol viscosity as a function of temperature between 0 to 100°C. At

21.9°C, the propylene glycol is expected to show a viscosity of 47.1 cP. Again, with standard deviation of 0.32 cP, the Brookfield viscometer is highly precise.

With the precise measurement and appropriate usage of the Brookfield viscometer, the fluid viscosity of the nanofluid can be measured at different temperatures. With the Vol.% dependence caused by the nanofluid particles, the viscosities are expected to increase from water, the suspension solution.

Section 3.4. SILICA NANOFLUID PROPERTIES

3.4.1. Literature and Interest

There has been significant interest in investigating nanofluids for enhancing liquid thermal conductivity and viscosity. Nanofluids contain either metallic or nonmetallic additives nanoparticles in base fluids such as water. Because the dispersed nanoparticles possess better thermal conductivity at solid state, it is hypothesized that nanofluids could have better thermal conductivity than the base fluids. Generally, the dispersed particles sizes are smaller than 100 nm.

Silica, or silicon dioxide (SiO_2), is an oxide crystalline solid with low electrical conductivity and no magnetic behavior. Its compact crystalline structure allows the solid to form into small nanoparticles dispersed in water without short-term settling. The bulk solid silica thermal conductivity is 1.38 W/m-K Ref. [4], significantly higher than liquid water. The bulk solid density ρ_p is between 2200 to 2300 kg/m^3. Its specific heat energy c_p is 745 J/kg-K.

3.4.2. Procurement and Preparation

The nanofluid tested in this study is a LUDOX® TMA colloidal silica suspension with 34 percent weight (%Wt) in water. The nanofluid is purchased in bulk from Sigma-Aldrich in 4 liter polymer bottles. According to its distributor specifications, the nanofluid has a pH between 4~7. The approximate particle diameter is 20 nm. Most important measure of the

nanofluid is its density, at 1.23 g/mL at 25°C. This measure allows calculation of volume percent, which is useful in dilution and thermophysical property correlation calculation.

For thermophysical properties measurements, the nanofluid was drawn in small samples. Safety procedures were used to ensure personal protection although the nanofluid is not hazardous. The silica nanofluid was drawn from the distributor container using 25mL syringe suction. For samples containing a lesser concentration, the nanofluid is diluted according to volume percent. Volume percent, or ϕ, is calculated from the percent weight (w) concentration and the thermophysical properties of both the base fluid and the nanoparticles suspension Ref. [17],

$$\phi = \frac{w\rho_w}{\rho_p(1-w) + w\rho_w}. \tag{11}$$

This equation is used to translate the bulk percent weight concentration (34%Wt.) to 18.6Vol.% volume concentration. In this experiment, deionized water is added to the nanofluid for dilution.

3.4.3. Nanofluid Stability Tests

Qualitative observations are made for the silica nanofluid to determine its stability under higher temperature conditions observed in the fluid flow loop. Because the chilled water is maintained at constant temperature, the heat transfer inside the accumulator decreases as flow rate increases. Thus, steady state bulk inlet and outlet temperatures are higher for experiment parameters involving higher flow rates.

The silica nanofluid was heated on a hot plate in a glass beaker to observe physical changes at various temperatures. Since the experiment only involves single-phase liquid, the maximum temperature of the nanofluid was 100°C. The silica nanofluid at 34 Wt.% is observed as stable and physically unchanged until the temperature reaches ~80°C. At this temperature, the silica nanoparticles agglomerate, creating a thin layer of white solid at the top of the fluid sample. The agglomeration is not desired in the heat transfer experiment. Particle agglomeration implies the colloidal dispersion is unstable, as well as creating solid residues in the experimental loop that can be difficult to clean.

Section 3.5. FLUID PROPERTY TESTS AND RESULTS

3.5.1. Thermal Conductivity

Using similar procedures with base fluid property measurements, the thermal conductivity and fluid viscosity were measured. Using the KD2Pro conductivity probe, the thermal conductivity is taken in 10 successive measurements, with 15-minute intervals that allow the fluid and probe to come into thermal equilibrium. Two samples were measured: one at 34 Wt.% (18.6 Vol.%) and another at 9.3 Vol.%. The 9.3 Vol.% is prepared with approximately 25 mL silica nanofluid and 25 mL deionized water. The samples are stored in 50 mL BD Falcon plastic centrifuge tubes.

The silica nanofluid at different concentrations show different thermal conductivity behaviors. At 18.6 Vol.%, the average thermal conductivity for ten data points is 0.670 W/m-K, with a standard deviation of 5.66×10^{-3} W/m-K. At 9.3 Vol.% nanofluid sample, the average thermal conductivity is 0.634 W/m-K, with a standard deviation of 9.49×10^{-4} W/m-K.

The results from the KD2Pro instrumentation study is compared to theory widely used to estimate the thermal conductivity of water-based suspensions. Using the Maxwell-Garnett model Ref. [19], the thermal conductivity of the nanofluid (k^*) can be calculated as a function of the water or base thermal conductivity (k_1) and the volume percent concentration,

$$\frac{k^*}{k_1} = 1 + \frac{3\phi(k_2 - k_1)}{k_2 + 2k_1 - \phi(k_2 - k_1)}. \tag{12}$$

The bulk solid thermal conductivity of silica is represented in k_2. The Maxwell-Garnett expression assumes that the nanofluid particulates are randomly oriented and monodisperse isotropic spheroids.

With the Maxwell-Garnett model in mind, the thermal conductivity quotient of the nanofluid suspension to base water is obtained from the data results. The measured average ratios for 18.6 Vol.% and 9.3 Vol.% are 1.102 and 1.045, respectively, taken

between 24.26°C and 25.19°C. With the addition of the temperature dependent liquid water thermal conductivity, as modeled with to the fourth-order polynomial curve fitting method, the theoretical ratio can be determined for the Maxwell-Garnett model. It is found that the average ratio for the similar range of temperatures is 1.176 and 1.086, for 18.6Vol.% and 9.3%Vol concentrations, respectively. The error between theory and measurement is 6.3% and 3.7% for the respective concentrations. These values are well within range.

3.5.2. Fluid Viscosity

The fluid viscosity is measured using the Brookfield Cone and Plate (C/P) LVDV-II torque viscometer, capable of measuring viscosities as low as 0.1 cP (0.0001 Pa*s). Both nanofluid samples are put into the holding cup, containing fluid samples of 0.5 mL. A hot water bath is also used to control the temperature of the fluid. The test matrix involves testing each sample at incremental temperatures of 5°C. Measurements stopped when the nanofluid agglomerates as fluid viscosity increases with rising temperature. The approximate temperature of nanofluid at which viscosity begins to increase is marked as the temperature of agglomeration. The fluid viscosity reading measurements from 18.6 Vol.% and 9.3 Vol.% silica nanofluid are plotted with temperature in Figure 3.6.

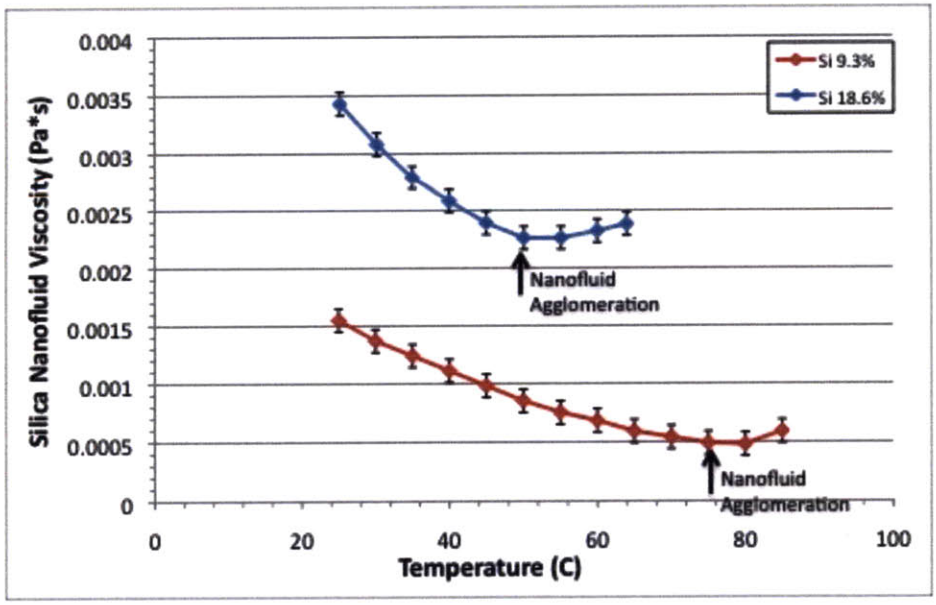

Figure 3.6. Plot showing the viscosity of silica nanofluid using Brookfield viscometer

The plots show that the viscosity of the nanofluid at higher volume concentration behave with higher fluid viscosity. For example, at approximately ~30°C, the nanofluid at 18.6 Vol.% has a viscosity of 3.08 centipoise (3.08×10^{-3} Pa*s), whereas the nanofluid at 9.3 Vol.% has a viscosity of 1.37 cP (1.37×10^{-3} Pa*s). This is obervation of higher nanofluid viscosity with increasing concentration is consistent with other studies.

Further observations can be made from the torque viscometer results. It is observed that the nanofluid agglomerate at lower temperatures for higher particle concentrations. The viscosity begins to increase as the water bath temperature exceeds ~55°C for 18.3 Vol.% silica. The lower concentration silica nanofluid agglomerates at ~80°C, as the viscosity begins to rise as this temperature.

The above figure also shows how the fluid viscosity behavior can be modeled. Using a fourth-order polynomial curve fit method, the equations seen closely fit the curve demonstrated by the data points. This may be useful in ultimately determining fluid viscosity at discrete temperatures for calculation and analysis.

3.5.3. Colloid Density

Since the silica nanofluid has particle sizes between 20 to 100 nm, it is classified as a colloid, or a homogeneous liquid mixture. For this specific nanofluid, the two ingredients are a silica nanoparticulate solid and liquid water. The combination of solid particles in a liquid is a sol, much like blood or ink.

Typical colloidal suspensions will settle and agglomerate over time, i.e. hemoglobin separates from the plasma in undisturbed blood. The aggregation is attributed to the inter-particle forces such as van der Waals interactions, electrostatics, entropy, gravity, etc. To partially overcome these interactions, chemical surfactants are used to coat the nanoparticles at their surface. The surfactants are usually in the form of a layer consisting of a hydrophobic head and hydrophilic tail. These surfactants are able to able to maintain a small constant electrostatic charge that repels similarly-charged particles. Thus, the silica nanofluid is able to exist as a homogenous solution that does not agglomerate over time.

For a suspended hydrocolloid, the overall nanofluid density Ref. [17] can be estimated for heat transfer analysis. The nanofluid density (ρ^*) can be given in relation to the volume percent concentration of the nanofluid as well as the respective densities of the solid (ρ_p) and base liquid water (ρ_w),

$$\rho^* = \rho_p \phi + \rho_w (1 - \phi). \tag{13}$$

The surfactant that coats the nanoparticles are ignored in density calculation because the molecular weight compared to the SiO_2 solids is small.

3.5.4. Specific Heat

The specific heat energy is the energy needed to increase the temperature of a body. With the assumption developed for the silica nanofluid as a homogeneous hydrocolloid, heat addition to a single-phase liquid should be in thermal equilibrium. The liquid and solid suspension should respond to heat as a single body of fluid. The specific heat (c^*) of the system can be calculated as Ref. [17],

$$c^* = \frac{c_p \rho_p \phi + c_w \rho_w (1 - \phi)}{\rho^*}. \tag{14}$$

Where the specific heat of the silica particle (c_p) and water (c_w) can be determined from the table of thermophysical properties (Table 3.2). The specific heat of the base fluid, water, should be correlated to the respective fourth-order curve fit model of water.

CHAPTER 4. DESCRIPTION OF EXPERIMENTAL FACILITY

Section 4.1. EXPERIMENTAL APPARATUS

The fluid flow loop used to characterize the nanofluid is located in the Nuclear Reactor Laboratory Green Lab. Many apparatus components are legacy parts from the past experiment run by an undergraduate student Ref. [16]. The original configuration was designed for solely laminar flow domain, with its differing component being the pump. For this experiment, new components are implemented to obtain the desired single-phase and flow rate characteristics.

A schematic of the current experimental apparatus is shown in Figure 4.1. A recent photograph of the fluid flow loop is shown in Figure 4.2.

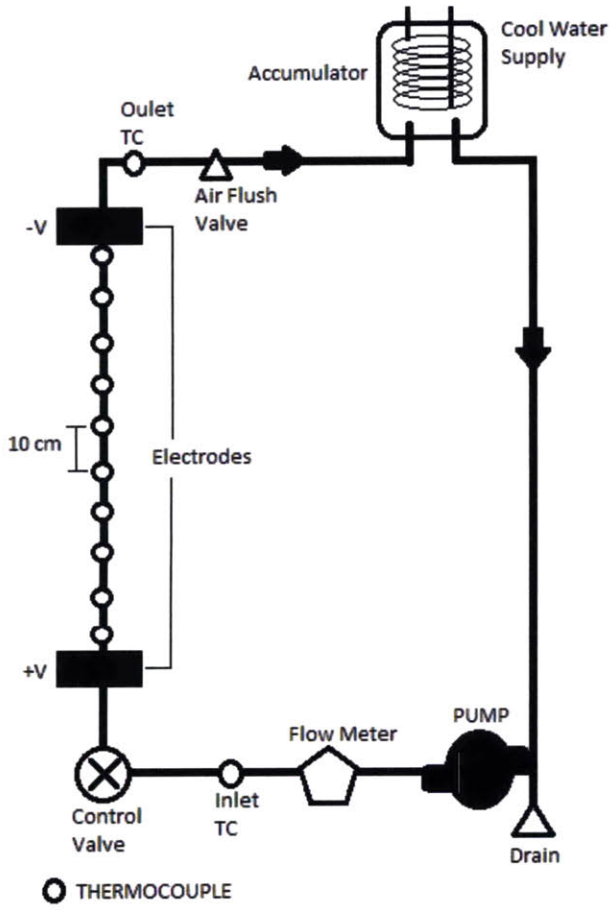

Figure 4.1: Schematic of the flow loop

Figure 4.2: Flow loop experiment apparatus

The following sections describe the critical components pointed out in the schematic.

4.1.1. Power Supply

To provide a constant heat flux across a heated fluid test section, a high-voltage DC power supply is used. A Lambda Genesys™ 20V-500A AC-to-DC power supply (Figure 4.3) is implemented for this experiment. Its rated power is 10 kW, with maximum outputs of 20 V and 500 A. The power is delivered to the test section using copper electrode blocks that are fixed onto heavy-duty electrical cables. The distance between the copper electrodes provide resistive heating to the test section tubing.

Figure 4.3: AC/DC power supply

The temperature increase of the fluid can be derived from fundamental heat conservation equations, in the form of,

$$T_{OUT} = \frac{1}{c_{p,OUT}}\left(\frac{Q}{\rho(T)v_f A} + T_{IN}c_{p,IN}\right). \tag{15}$$

The equation assumes that the fluid properties change as a function of temperature. Here in this case, the specific heats c_p are different at the inlet and outlet of the heated test

section. Although the fluid density is temperature-dependent, it can be simplified to the average value through the test section since the nanofluid density change is small at the operating ranges of interest. Note that temperature difference increases as the power input from the supply is increased. The fluid flow velocity v_f also greatly affects temperature changes. The following section describes how the fluid flow rate is determined.

4.1.2. Gear Pump

The pump configuration used in the Rea experiment has limited flow rates because the fluid is impelled using two internally meshed plastic gears. The finned-aluminum 12V-DC low-flow miniature gear pump, as seen in Figure 4.4, only has flow rate capability up to 0.61 gpm Ref. [12]. Thus the gear driven pump is used primarily for laminar flow experiments only. To achieve a higher flow rate and greater range, a new 120V-AC centrifugal pump is needed for the experiment.

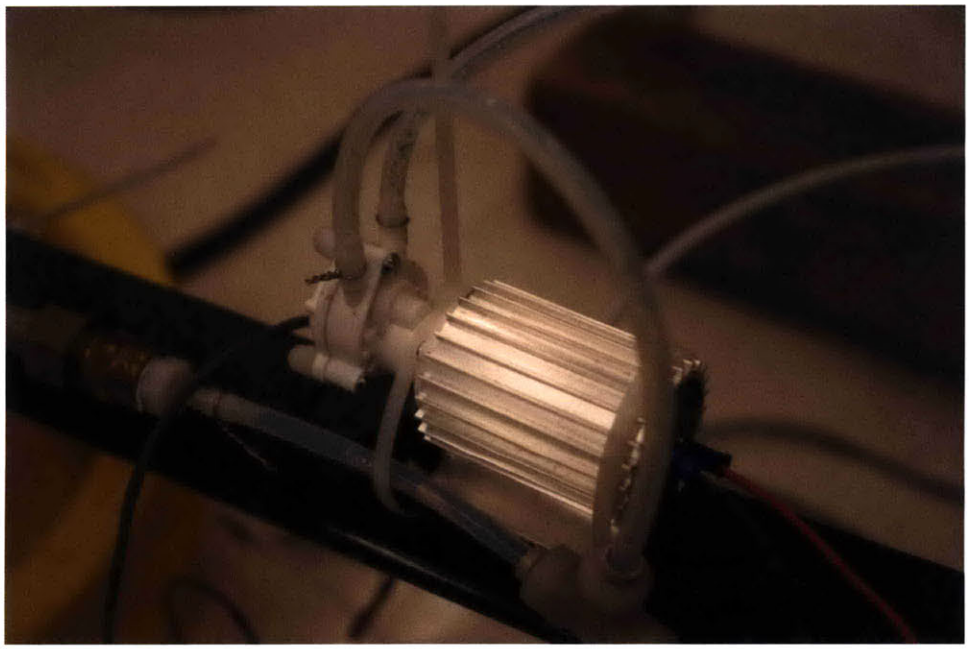

Figure 4.4. 12V DC water gear pump

A new pump acquired was an Oberdorfer Model 142-01A46 plastic centrifugal water pump. At optimum efficiency, the pump delivers approximately 0.7 gallons per minute for pure deionized water. This pump would ideally be able to deliver both laminar and

turbulent flow conditions. However, because the pump operates for high-pressure heads, air traps can form from tube fittings upstream of the pump. With initial water test validation, it was found that the heat transfer coefficients do not match well against laminar and turbulent flow correlations. The original miniature gear pump was reinstalled for testing.

4.1.3. Flow Meter and Throttle Valve

The throttle needle valve downstream of the pump is primarily used to control the flow rate of the fluid inside the experimental apparatus. The valve is just before the elbow and upstream from the heated test section. For turbulent experiments where developing length is brief, the valve is frequently used.

To measure the fluid flow rate, an Omega FTB9504 flowmeter is used (Figures 4.5). The flowmeter utilizes a Pelton paddle-wheel rotor whose motion is measured by a pickup coil Ref. [14]. The flow rate is output as a proportional frequency. The frequency to Reynolds number or mass flow rate correlation is obtained from timed water release calibrations at constant temperature. Calibration results are also shown in Figures 4.5. Omega also provides a 20-point calibration curve that can determine the correlation between rates. The instrument measurement uncertainty is ±0.5%.

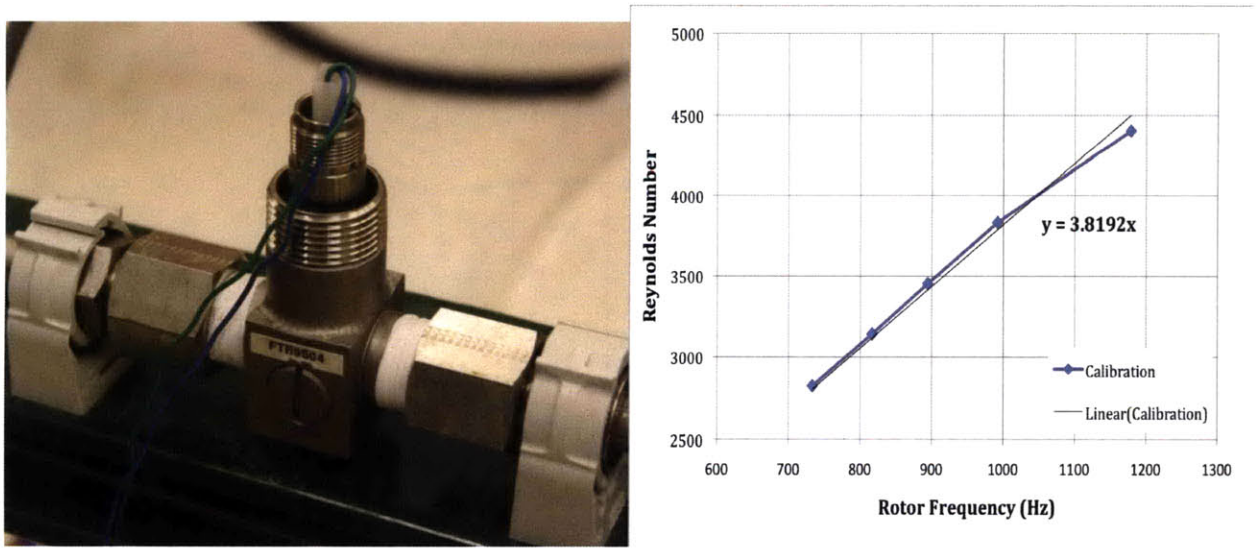

Figures 4.5. (a) Paddle-wheel type flowmeter, and (b) its data acquisition calibration.

4.1.4. Thermocouples

To measure the temperature of the fluid as well as outer wall temperature of the heated test section, thermocouples are used to simultaneously acquire the states. The thermocouples are standard K-type thermocouples, made from nickel-chromium and nickel-aluminum alloys in each lead Ref. [15]. The common K-type thermocouple has a temperature range between -200°C to 1250°C. Its standard limit of error is ±2.2°C or ±0.75% whichever is greater.

The thermocouples that probe the inlet and outlet fluid temperatures are implemented differently than the wall-mounted probes on the heated test section. The thermocouple probes are inserted into a Viton-sealed compression tube tee fitting. The thermocouple probe tips measure the temperature of the fluid at its approximate center of flow.

4.1.5. Heated Test Section

The heated test section is constructed using 316 stainless steel tubing. The outer and inner diameters are selected at 0.25" and 0.218" respectively. The heated test section was constructed at around 1.6m in total length. The thermocouples are evenly distributed across the heated section, spaced apart at 0.1m between the two copper electrodes. The thermocouples are attached to the surface using plastic loop clamps. Since there are limitations of thermocouple uncertainties, the temperature difference between inlet and outlet bulk fluid temperature should be as large as possible. The bulk temperature difference is considered during operating procedures using the power supply.

From Section 3.1, the entry length is taken in consideration due to the developing laminar flow. Due to the temperature parameters set for the experiment, the entry length is reevaluated as Ref. [3],

$$L_{e,T} = \frac{\mathrm{Re}\,\mu c_p \Delta T_b}{4q''}. \tag{16}$$

Note that the relation is dependent on bulk temperature difference (ΔT_b). Taking into account for both relations, at corresponding Reynolds numbers, the entry length is

between 0.4m to 0.6m for ΔT_b = 20°C. The 1 meter long heated test section from electrode-to-electrode should be sufficient for seeing fully developed flow.

4.1.6. Accumulator/Cool Water Bath

The accumulator/cool water bath is a heat exchanger that maintains steady inlet bulk fluid temperatures during experiments. The heat exchanger is made of coiled copper tubes. The coiled tubes are placed inside a plastic container capable of holding storing more than 3 liters of fluid. A purpose of the reservoir is to eliminate air bubbles created by pressure vacuums inside the fluid flow loop sections. Figure 4.6 shows the cool water bath apparatus.

Figure 4.6. ~400 mL accumulator and cool water bath

4.1.7. Differential Pressure Transducer

The differential pressure transducer is used to measure pressure drops between two points of the test loop. The pressure head required to pump fluids at certain mass flow rates is determined using this device. The DPT is an Omega PX154-001DI. The DPT in this experiment measures the difference in pressure between the cool water reservoir and the pump inlet/water drain, at a length comparable to the heated test section. The actual DPT in this experiment did not work. The inlet fluid nozzle was found to be blocked by possible sediment. No fluid was measured by the DPT.

4.1.8. Data Acquisition System

The DAS used is an Agilent Technologies 34980A Multifunction Switch/Measure Unit. It is capable of measuring more than 40 channels of digital data. The software used to acquire data from the configurable card is BenchLink Data Logger. Figure 4.7 shows the DAS during an experiment. The configurable channels used in this experiment measures several channels of thermocouple temperature, flow meter frequency, power supply voltage and current and DPT current. Calibrated constants can be provided to view real-time properties.

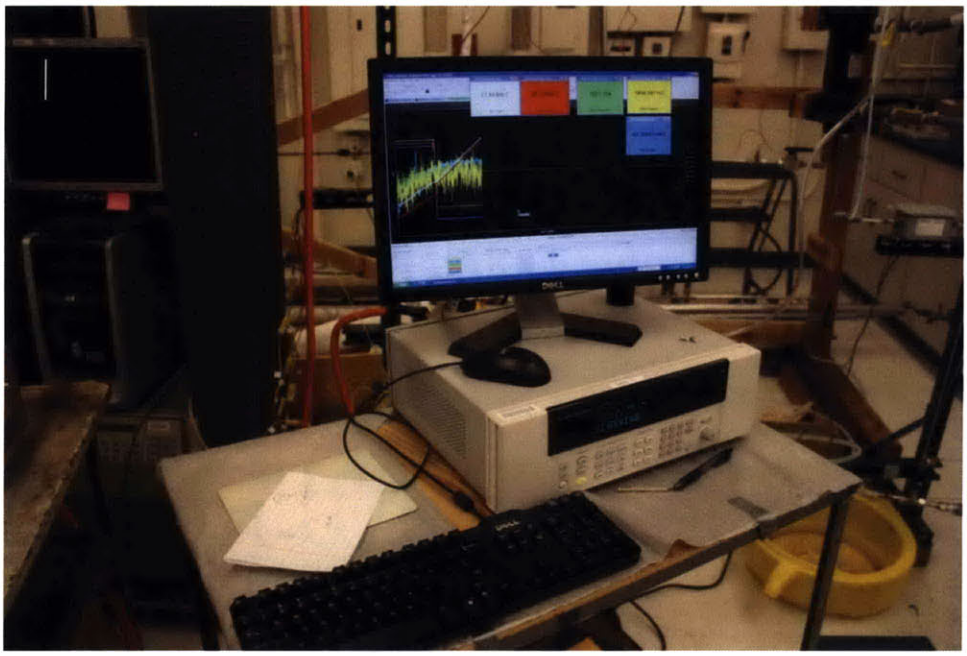

Figure 4.7. Data acquisition system

Section 4.2. FLOW LOOP PROCEDURES

4.2.1. Preparation

1. For testing the thermophysical properties of any fluid, the materials described in the previous section are used to begin the experiment. Before obtaining any fluid, the fluid flow loop must be prepared: The flow loop is checked to see if all components are in

good shape and no signs of tampering or damage. The drain valve should be in the off position. The t-valve used for fluid flushing should be in the direction that completes the fluid loop. The heated test section inlet valve should be in the full open position.

The power supply is checked to be NOT on and unplugged. The pump power cord should also be unplugged. The DAS is acquired and the reader card is attached to the multichannel unit. In the BenchLink, make sure no data is read.

2. Begin acquiring fluid. For water, approximately 2.5 liters is acquired from a water deionization unit in the lab. The 2.5 liters is put into the system at around 1 liter a time using a flask.

   For the silica nanofluid, the distributor container is brought to the fume hood to isolate it and protect the laboratory from accidents. The silica nanofluid is diluted to [X] Vol.% in water. The nanofluid dilute has approximately same volume as experiments with water.

3. The accumulator is filled with the fluid of interest. For safety, the first half liter is slowly filled into the accumulator because the first sight of leaks can then be detected and controlled. Pour the remaining fluid into the accumulator while visually checking to see the fluid fill the clear pipes leading into and out of the pump.

4.2.2. Flow Loop Operation

1. Now, make sure that the fluid has completed settled and no issues arise. Plug in the power cord for the pump. Turn on the pump at maximum speed. Let the pump run at this flow rate/speed for approximately five minutes. Observe whether the clear tubes for the pump inlet and outlet have bubbles, or that the sound of the pump does not fluctuate.

2. Heating the test section can begin. Plug in the cord for the power supply into the wall outlet. Turn on the power supply. Make sure that the LCD display reads "OFF." Then, press the "OUT" button. Because the power supply stores the power output from the previous experiment or user, the power output may not be zero. Turn both knobs

counterclockwise to reduce both voltage and current to make sure no power spikes occur to the test section.

3. With the power set to zero and the fluid running at steady flow rate, begin acquiring data. BenchLink allows storage of channels for different experiments or users. With the channels used and configured in this experiment, run the data acquisition for indefinite time (until the user presses "stop") at a sampling rate of one per second. Observe the trends of the channels—if a channel does not display a reasonable value or has no reading, stop the system and troubleshoot.

4. The power supply can now be gradually turned to increase power output. The power output will be shown both on the LCD displays on the unit as well as channel data on the DAS. The readings on both parts should be approximately the same, or else losses or shorts are disturbing the system. For a typical water-based fluid at liquid phase, the current output should be increased at incremental units of around 20A. ~10-20A increments are introduced when the outlet and inlet temperatures on the DAS are observed to be relatively stable.

5. Before reaching maximum power, it is made sure that the accumulator/chiller is turned so that the temperature does not rise too high. Typically, the cold water supply is switched on when the output current rises above 50-60A. The effect of the cold water supply is observed on the DAS when the outlet and inlet temperatures decrease.

6. When the power output is set such that an appropriate bulk ΔT is read between the inlet and outlet, the system is waited to settle to fluid heat exchange equilibrium. This time varied between 10 to 30 minutes.

7. During equilibrium, the DAS is stopped. The acquisition time is set to 3 minutes, or 180 data points. The data acquisition begins. The data sampling stops automatically and the data are saved into a format readable by Excel spreadsheet.

4.2.3. Post-Experiment

1. Experimentation ends when sufficient data points are acquired. To prepare for shutdown, the power supply is dialed down to zero, turned off and unplugged from the wall outlet. This ensures that the fluid does not overheat when the fluid stops running.
2. Turn off the pump and unplug cord from the outlet.
3. The cool water for the accumulator is turned off.
4. Return all valves to the original positions described in the preparation. Once this is done, the drain valve is opened and the fluid is poured into a suitable plastic container/bucket. The fluid flush t-valve is opened to allow air to purge the system of fluids.
5. *If the system ran with nanofluid, the system is run again with deionized water to rinse the loop of residues. Water is run with the above procedures except the presence of power supply.
6. Area cleaned out and the flow loop visually checked for damage or problems.

CHAPTER 5. HEAT TRANSFER CHARACTERISTICS RESULTS

Section 5.1. WATER VALIDATION TESTS

Before subjecting nanofluids into the flow loop apparatus, it was necessary to test experimental equipment with deionized water to ensure that all instruments are working properly and the heated test section behaves according to theory. The system was given 3000 mL of deionized water. The pump was run at five different flow rates, controlled by positioning the inlet valve. The Reynolds numbers of the flow rates are all under Re = 2300, such that the system runs in laminar regime. For the deionized water experiments, the flow rates and their respective Reynolds numbers are shown in Table 5.1.

Flow rate (gallons/minute)	Inlet Reynolds number
0.0492	777.58
0.0581	917.66
0.0697	1100.35
0.0766	1210.30
0.0833	1314.11

Table 5.1. Flow rates and respective Reynolds numbers at inlet for deionized water experiments.

The above table shows the respective behavior of the fluid at the inlet of the heated test section. The Reynolds number obtained from the data acquisition system represents only the flow rate at the flow meter, or inlet. The Reynolds number is affected by several changing fluid properties, as seen in Eq. (3). Thus, heat transfer calculations were based on instantaneous Reynolds numbers based on local temperature of the heat test section. The temperatures at the inlet for the deionized water experiments range from 14.4^{o}C to 17.2^{o}C. With the inlet to outlet temperature difference set at an approximate 20^{o}C, the outlet temperatures range from 35.0^{o}C to 37.7^{o}C, in similarly increasing order. The bulk temperature, or average temperature in the gradient of the moving fluid, is calculated as linear increments divided equally between the inlet and outlet temperatures, distributed at the location of the thermocouples.

The Nusselt number, as mentioned in 3.1.3, should be Nu = 4.36 for deionized water running at any fully developed laminar flow in a pipe with constant wall heat flux Ref. [10]. However, part of the heated test section is situated in the developing region. The entry length is defined in Eq. (6). With this relation, Reynolds number is changing as the fluid is passed through the pipe. Thus, the "entry length" changes down the heated test section. With increasing bulk temperatures the definitive entry length can only be approximated. The start of the region of fully developed laminar flow ranges between 0.3m and 0.5m from the inlet.

Thus, a Nusselt correlation developed by Lienhard [10] satisfies local entry flow conditions in laminar regimes,

$$Nu = 4.364 + 0.263\left(\frac{x_+}{2}\right)^{-0.506} \exp\left(-41\frac{x_+}{2}\right). \tag{17}$$

Nusselt numbers taken from the heated test section experiments are plotted against a dimensionless distance x_+, as defined as,

$$x_+ = \frac{2x}{D_i \mathrm{Re}\,\mathrm{Pr}}. \tag{18}$$

After calculating the Nusselt number correlations, Figure 5.1 shows the plot of Nusselt number versus the dimensionless distance in the deionized water experiments.

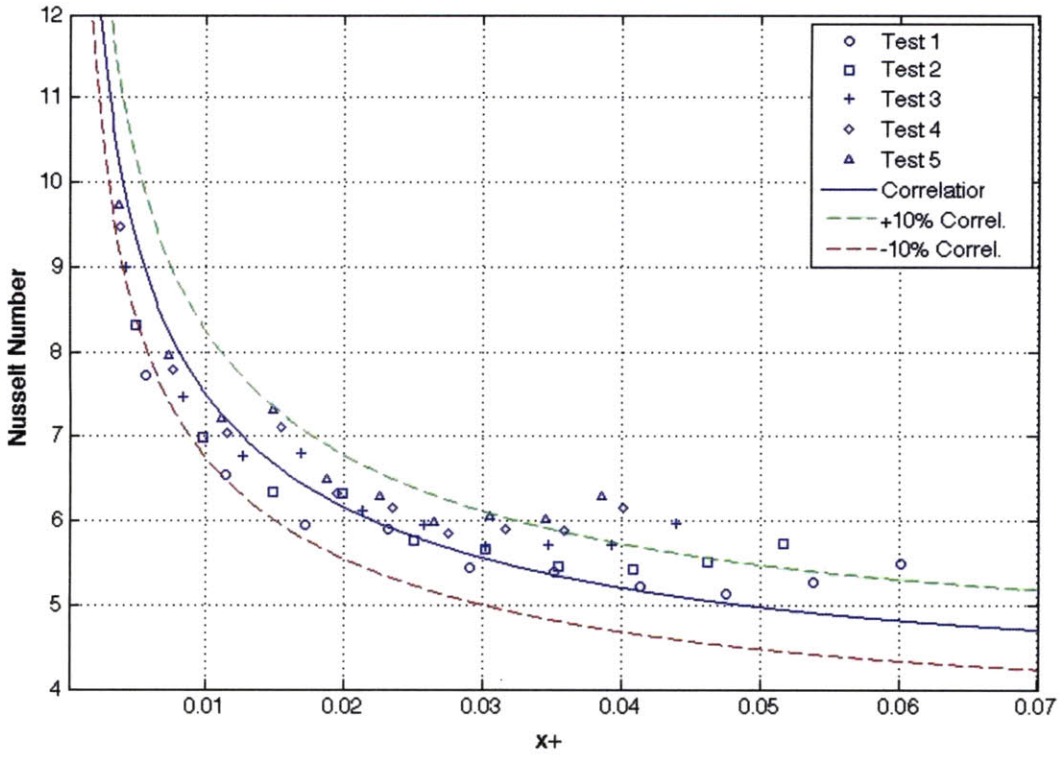

Figure 5.1. Nu versus x_+ data points in heated test section using deionized water. Lienhard correlation solid line with dashed ±10% error lines.

The Nusselt numbers decrease with distance from the inlet of the heated test section. The behavior can be visually fitted to a power-exponential curve. The initial data (black crosses) show that the correlation is well below the experimentally observed behavior.

This is attributed to the calculation of the power consumed by the heated test section. The data on power consumption is based on the voltage and current measured within the power supply ($P = VI$). This does not account for the heat loss due to atmospheric and environmental convection and conduction. Thus, the more accurate quantification of the power consumption can be calculated using,

$$P = \dot{m}(c_p T_B)\Big|_{in}^{out} \tag{19}$$

The experiments involving the deionized water has shown power losses between 7.86% to 11.93%.

Accounting for the power loss, the heat transfer coefficient is reevaluated. The blue dots in Figure 5.1 show that with this reduction, the data conforms more closely to the Lienhard correlation. To accurately compare the Nusselt numbers from the deionized water experiments, the predicted Nusselt numbers are compared to the measured Nusselt numbers. Figure 5.2 shows a plot comparing the two variables.

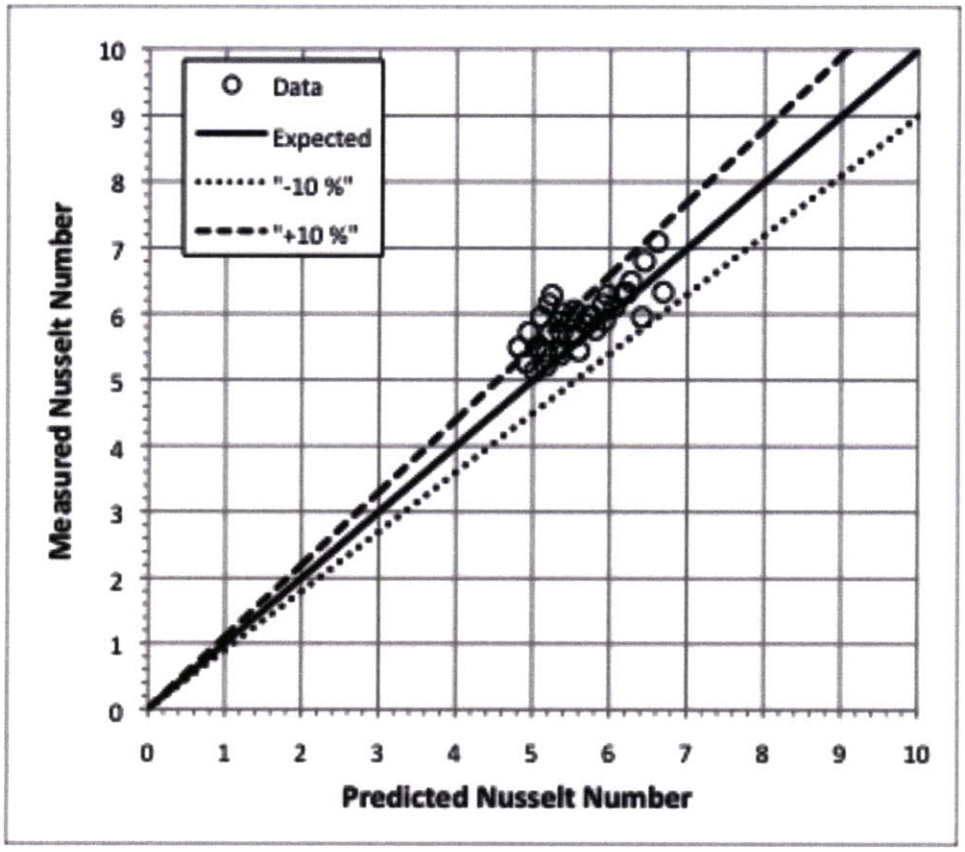

Figure 5.2. Plot showing comparison of measured versus predicted Nusselt numbers for deionized water tests.

The plot shows that most data points are situated close to the expected curve. A few points lie above the +10% curve, meaning measured Nusselt numbers are slightly higher. The higher Nusselt numbers could indicate that other heat losses still need to be mathematically accounted for, that these losses could in reality be above 10% due to external factors.

Section 5.2. SILICA NANOFLUID TESTS

The silica nanofluid was prepared by diluting the 34%Wt. (18.58Vol.%) solution into water. The concentrated nanofluid was pipetted into Florence flasks for accurate volume measurement. The volume of 34%Wt. silica (V_{nf}) needed is calculated using,

$$V_{nf} = \frac{C_{desired}}{0.1858} V_{TOTAL}. \tag{20}$$

The total diluted nanofluid volume (V_{TOTAL}) was 3500 mL for each experiment. Final percent volume concentrations ($C_{desired}$) of the tested nanofluids are 0.2%, 1%, and 5%. The flow rate is controlled in a similar manner to the deionized water tests. No Reynolds number corresponding to flow rate was above 2300 for any point.

Following experiments using silica nanofluid in the test apparatus, the nanofluid is drained then flushed with deionized water for more than 10 minutes. For each experiment, a sample of the nanofluid is kept in a test tube for future testing of the thermophysical properties. Table 5.2 details the parameters involved in each experiment in a test matrix.

ϕ	Flow rate [gpm]	T_{IN} (°C)	T_{OUT} (°C)	Re (Inlet)	q [W/m^2]	Q [W]	Heat Loss (%)
0	0.04921560	14.38817	35.04355	777.5773	17137.70	298.1960	11.92831
0	0.05808216	14.89020	35.04652	917.6628	19388.34	337.3572	9.953897
0	0.06965727	15.61786	35.54448	1100.352	22834.87	397.3267	9.244351
0	0.07663064	15.67939	36.03778	1210.298	25471.67	443.2070	8.439704
0	0.08325313	17.22481	37.68490	1314.113	27646.29	481.0454	7.860104
0.002	0.05324797	15.02985	34.81216	843.4795	17076.44	297.1301	7.751553
0.002	0.06577515	16.24064	37.00696	1041.115	22079.53	384.1838	7.525999
0.002	0.07581187	16.62674	36.28513	1200.290	24911.25	433.4557	11.15878
0.002	0.08944019	17.01786	37.21445	1415.589	29679.25	516.4190	9.299788
0.002	0.1016790	16.88133	36.71473	1609.584	32765.29	570.1160	8.065071
0.01	0.05451707	14.38377	34.44748	872.3958	17939.59	312.1489	9.521363
0.01	0.07663054	15.69464	35.02947	1226.022	24648.20	428.8786	11.11231
0.01	0.08979718	16.03952	36.03938	1436.181	28414.60	494.4140	5.712551
0.01	0.09806023	16.70552	37.09466	1567.758	32584.77	566.9751	8.933184
0.05	0.04872447	13.63207	33.94703	818.7289	17334.36	301.6179	19.79859
0.05	0.05567891	13.11799	33.05131	935.8351	18940.99	329.5733	16.70881
0.05	0.05983013	14.99228	35.86003	1004.749	21119.83	367.4850	15.79528
0.05	0.06637214	14.66472	34.83450	1114.966	22776.81	396.3164	16.42518
0.05	0.08160661	15.29681	35.14115	1370.756	27205.58	473.3771	14.96971

Table 5.2. Silica nanofluid heat transfer experiment test matrix.

The fluid flow loop first tested 0.2Vol.% silica nanofluid solution. The inlet mass flows set during these experiments are 0.0532, 0.0658, 0.0758, 0.0894 and 0.1017 gpm. These did not result in Reynolds numbers exceeding 2300 in any area of the heated test section. Similar methods were used to calculate and plot the Nusselt number versus dimensionless distance, which is shown in Figure 5.3.

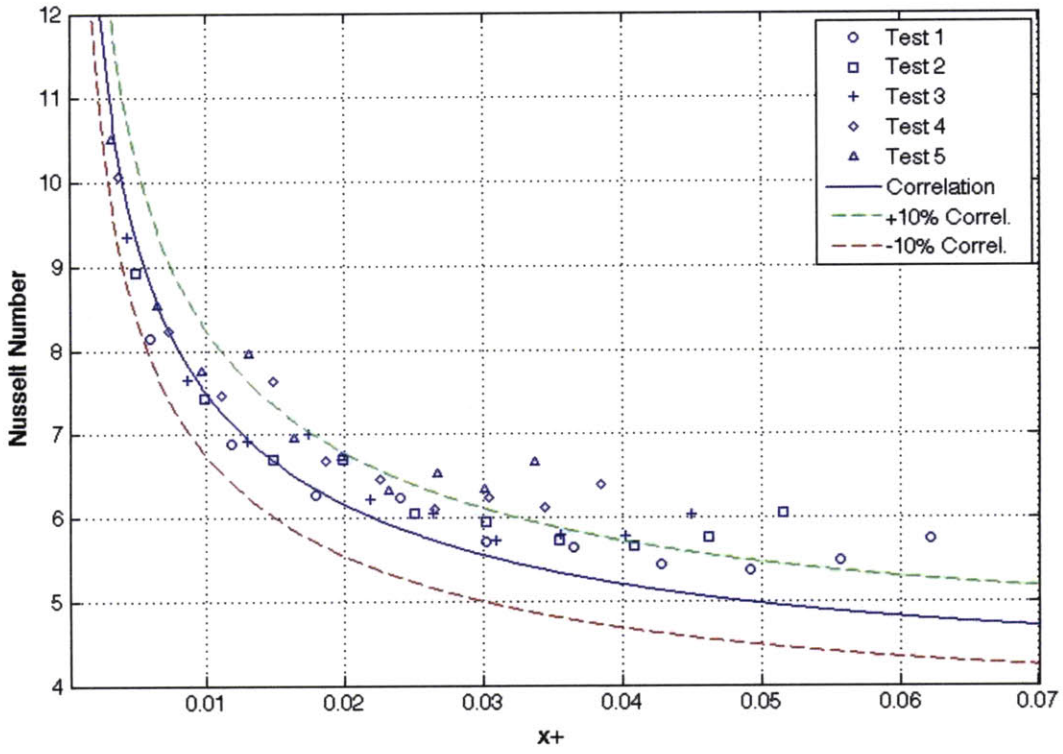

Figure 5.3. Nu versus x_+ in the heated test section with 0.2Vol.% silica nanofluid.

In the previous plot, it is observed that the Nusselt number close to the developed outlet is greater than Nu=4.36 value found in water. Yet, the data points lie mostly within the ±10% error margins for the correlation. Nusselt numbers at the outlet for each test are typically above correlation.

For the 1Vol.% solution, the inlet mass flows were set at 0.0491, 0.0545, 0.0766, 0.0898 and 0.0981 gpm. With the lowest flow rate, the flow meter output was not stable. The frequency that is read by the data acquisition fluctuated too greatly, which is typically more

than ±10%. The first set of the experiment was omitted in analysis. The Nu vs. x_+ plot of the 1Vol.% nanofluid test is shown in Figure 5.4.

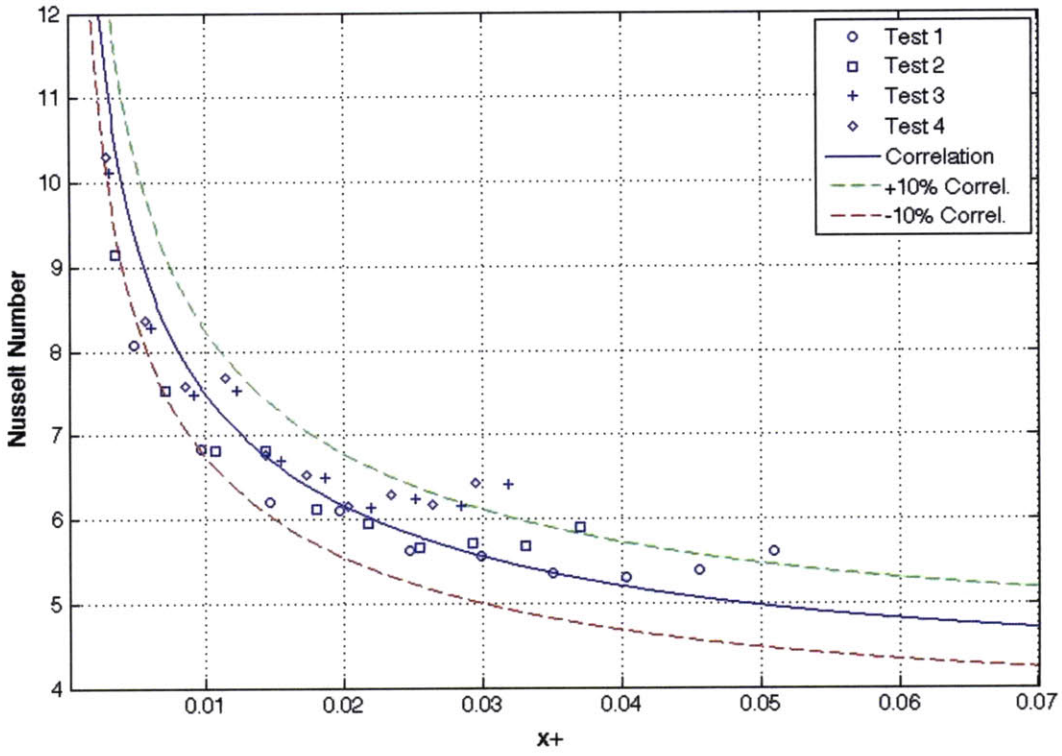

Figure 5.4. Nu versus x_+ in the heated test section with 1Vol.% silica nanofluid.

Finally, a higher concentration of silica nanofluid of 5Vol.% is tested in the experimental apparatus. The inlet flow rates for these sets of experiments were set at 0.0487, 0.0557, 0.0598, 0.0664, and 0.0816 gpm. It is noted that the stable flow rates for experiments consisting of higher nanofluid concentrations are typically lower. Nu vs. x_+ plot of the 5Vol.% nanofluid test is shown in Figure 5.5.

The Nusselt number data points, unlike those from the previous experiments, are well below the correlation line. By investigating the heat loss during the experiments, it was found that 15.0%, 16.4%, 15.8%, 16.7%, and 19.8% power was lost. Stable experiments typically have heat losses between 5-10%.

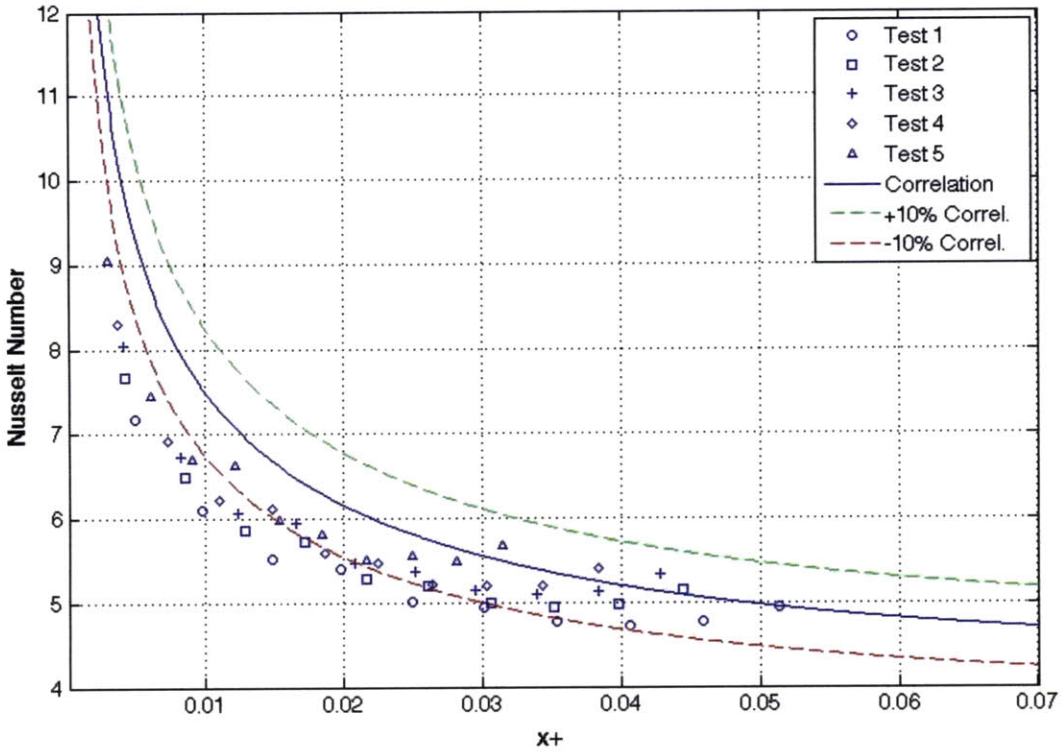

Figure 5.5. Nu versus x_+ in the heated test section with 5Vol.% silica nanofluid

Section 5.3. POST-TEST NANOFLUID PROPERTIES ANALYSIS

To analyze the thermophysical conditions of the silica nanofluids, post-test property analysis was conducted on small samples collected from the tests. The three concentrations of silica nanofluid are tested with the KD2 Pro thermal conductivity meter and the Brookfield viscometer. The methods of data collection are similar to the tests conducted as described in Section 3.4.

5.3.1. Thermal Conductivity Measurement

The thermal conductivity tests were conducted on each sample concentration ten times, and their results are plotted against their respective fluid concentrations in Figure 5.6.

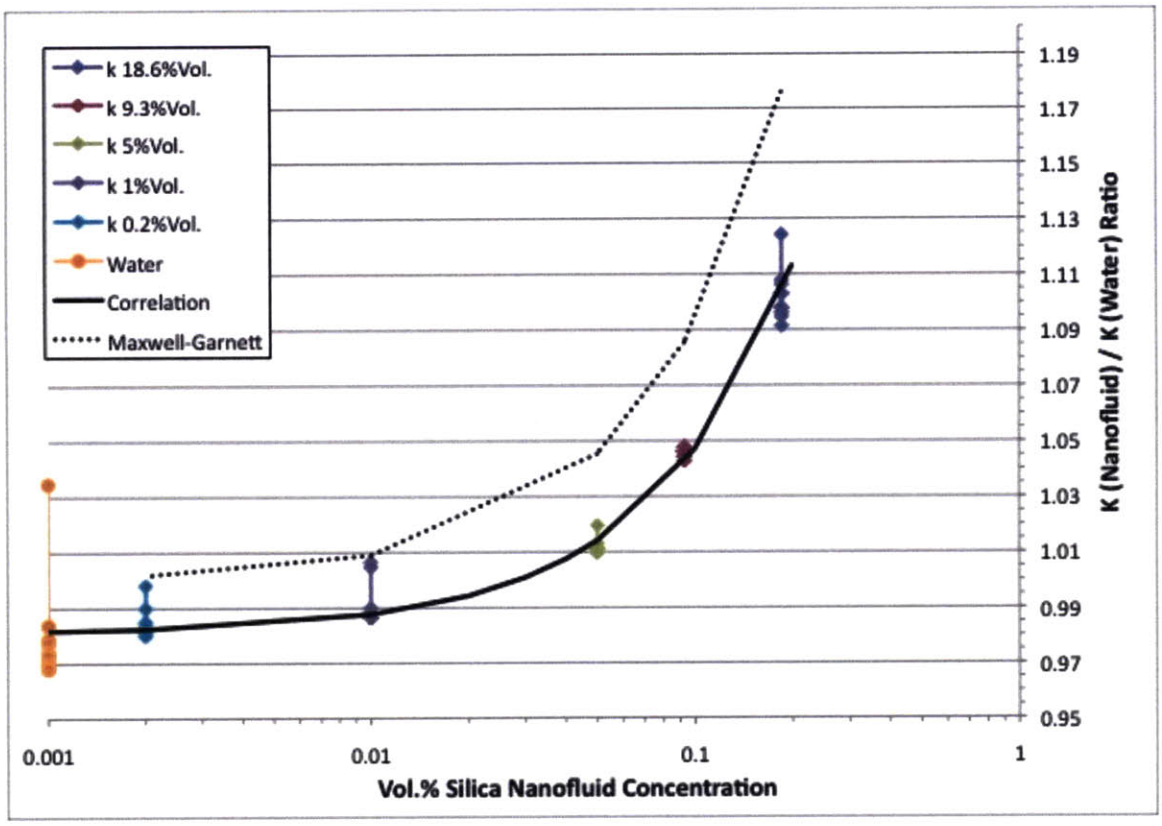

Figure 5.6. Thermal conductivity of silica nanofluid with respect to concentration at 25°C.

The plot shows that the thermal conductivity increases linearly with the percent volume concentration of the nanofluid. This is validated with the comparison to the Maxwell-Garnett model, which is shown to increase in a similar fashion. The slight offset from the Maxwell-Garnett model may indicate slight instrumentation or calibration error from the KD2 Pro sensor.

5.3.2. Viscosity Measurement

The viscosities from the samples were measured in the Brookfield viscometer in temperature ranges that correspond to what the nanofluid experiences while inside the heated test section. The temperature ranged from 25°C to 60°C (the water bath cannot be cooled below room temperature without external refrigeration). Figure 5.7 shows the thermal fluid viscosities trend with the temperature variation.

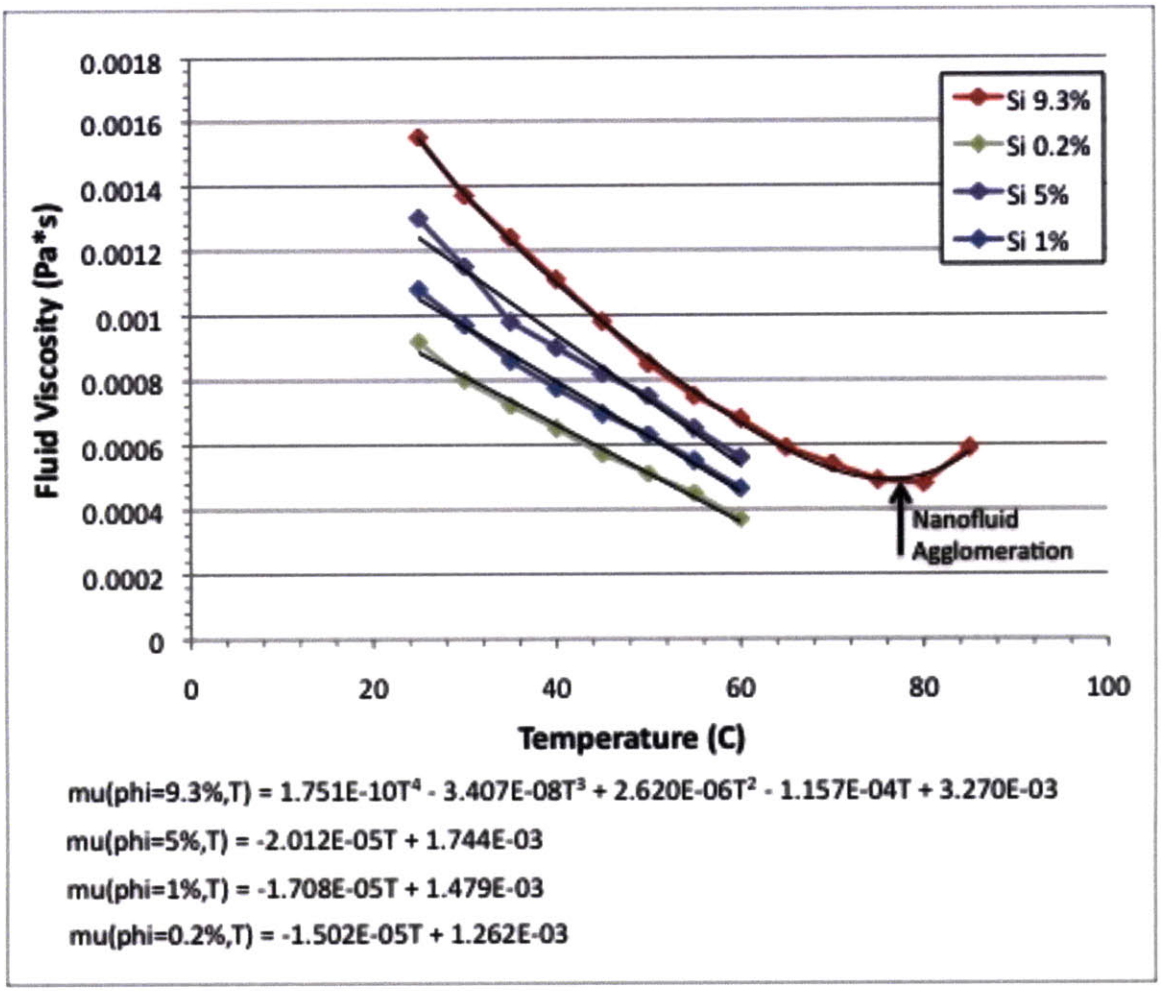

Figure 5.7. Silica nanofluid viscosity with increasing temperature.

From the recent temperature range, no agglomeration is observed, especially for samples with low concentrations of nanoparticles. In general, the viscosities decrease linearly with temperature. This is observed in the linear curve fits that are given in the Figure 5.7.

Subsequently, the fluid viscosities of the silica nanofluid are modeled with respect to nanofluid percent volume concentration. The Das group has modeled the viscosity of the 20nm particle diameter silica nanofluid with respect to percent volume concentration (ϕ) Ref. [6]. The formula for the nanofluid viscosity is given as,

$$\frac{\mu_{nf}}{\mu_{water}} = 1.092\exp(5.954\phi). \tag{21}$$

To compare their correlation to the readings obtained from the viscometer, the viscosities are plotted with increasing percent volume concentrations, as shown in Figure 5.8.

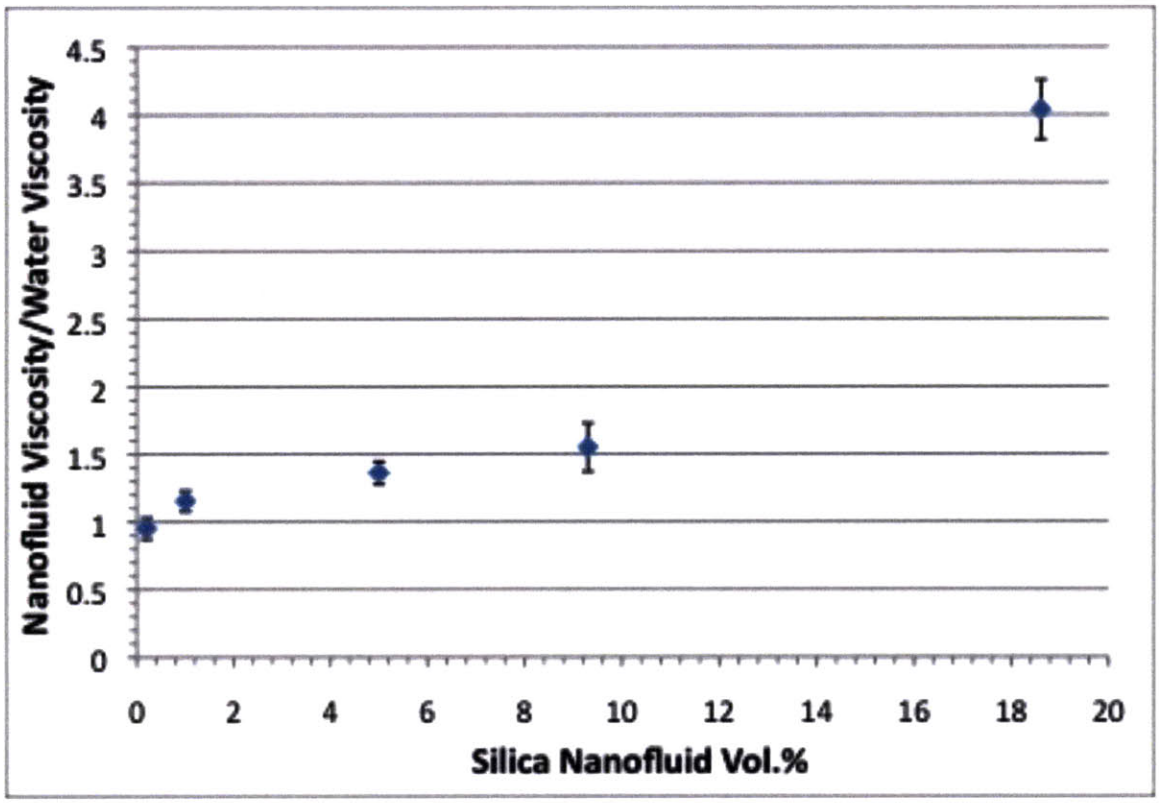

Figure 5.8. Silica nanofluid viscosity data with Vol.% concentration, with standard deviation error bars.

CHAPTER 6. DISCUSSION

Section 6.1. MEASUREMENT UNCERTAINTY ANALYSIS

The results revealing the Nusselt numbers at different areas of flows have a standard amount of uncertainty error. Uncertainty analysis performed by Williams reveals that during experimentation, limitation of instrumentation accuracy can cause propagation of differential error. For example, the error seen in the Nusselt number is calculated on MATLAB using the expression, Ref. [19]

$$\delta Nu = \sqrt{\frac{D_i^2}{k^2}\delta h^2 + \frac{h^2}{k^2}\delta D_i^2 + \frac{h^2 D_i^2}{k^4}\delta k^2}\,. \tag{22}$$

A discussion in Williams paper shows that there is ±10% error due to instrumentation. The sources of error consist of the ±1.1^{o}C variation in the thermocouple measurement. Also, the conductivity and viscosity measurement devices as well contain an inherent 1% error. Even the polynomial fit methods contain a small amount of error.

The propagated error of approximately ±10% means that any observation of increases or decreases enhancement of heat transfer is not significant. The correlation lines do not fall outside of this error margin.

Section 6.2. HEAT TRANSFER ENHANCEMENT FROM SILICA NANOFLUID

To determine the enhancement from the silica nanofluid, the average heat transfer coefficients from the three nanofluid experiments are divided by the average heat transfer coefficients from deionized water test. This ratio is plotted against the % volume concentrations of the silica nanofluid samples. Figures 5.9 show the heat transfer coefficient ratios in relation to the concentrations at the inlet and outlet of the heated test section.

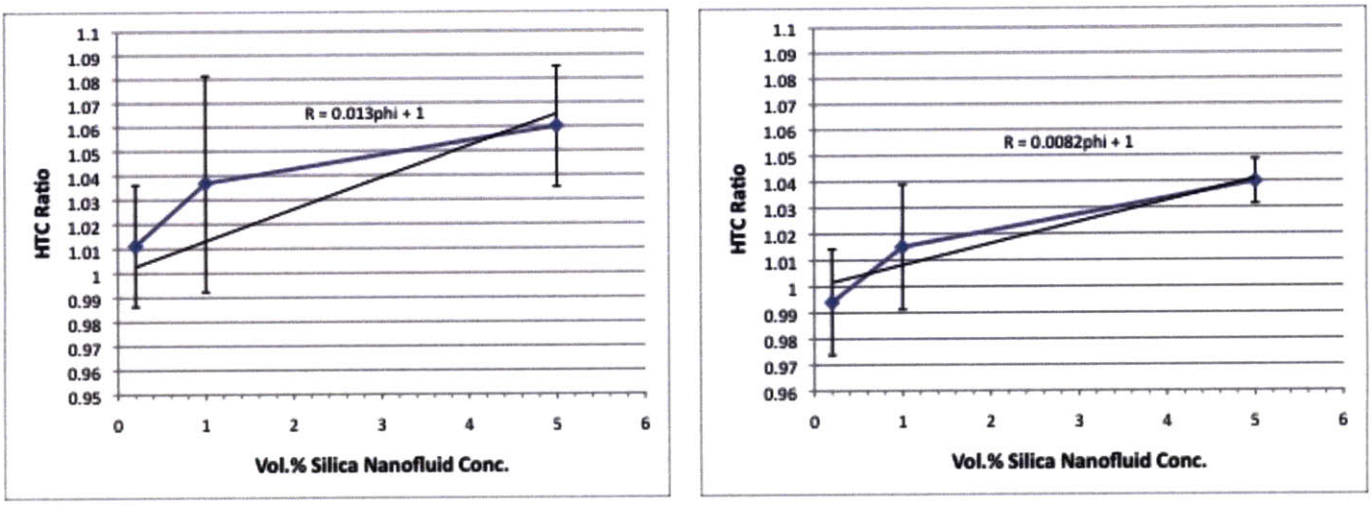

Figures 5.9. The heat transfer enhancement of silica nanofluid in varying concentrations at (a) the inlet of the heated test section, and (b) the outlet. Error bars of 1σ standard deviation.

Both plots show a slight increase in heat transfer with increasing concentrations. The outlet shows a slightly lesser rate of enhancement, as given by the slope difference from 0.013 to 0.0082. The 0.2 Vol.% experiment even showed a slight decrease in enhancement at the outlet, where the flow is fully developed. However, the observed increase of the heat transfer coefficient ratio has little significance. The data point containing tests involving 5 Vol.% silica nanofluid need to be omitted due to the high heat loss during these experiments (15% to 20%).

CHAPTER 7. CONCLUSION

The loop that was designed for the experiment successfully produced results that heat transfer coefficients of silica nanofluid in a single-phase laminar flow. The experimental apparatus was modified from a previous experiment. The loop was upgraded with ten new thermocouples to measure the outer wall temperatures. A new pump for laminar and turbulent experiments was briefly installed, but the physical parameters of the loop did not allow fluids to run at such high flow rates without drawing vacuum. The data acquisition capabilities were validated using heat transfer correlations and the tests conducted on deionized water.

Using the validation tests, experiments were conducted on samples of silica nanofluids of 0.2 Vol.%, 1 Vol.% and 5 Vol.% concentrations. At lower concentrations, there seem to be a slight enhancement; at higher concentrations, the coefficients are lower either due to thermophysical properties of the nanofluid or due to the excessive test section heat loss. There is a slight increase in heat transfer coefficient ratios as the concentration increases. However, these results have not been conclusive because they are within the experimental uncertainty. This agrees with the conclusions of previous studies that there is no abnormal heat transfer enhancement with oxide nanofluids.

APPENDIX

Section A.1. Plots on temperature dependence modeling of steam table water

Water Density (ρ_f)

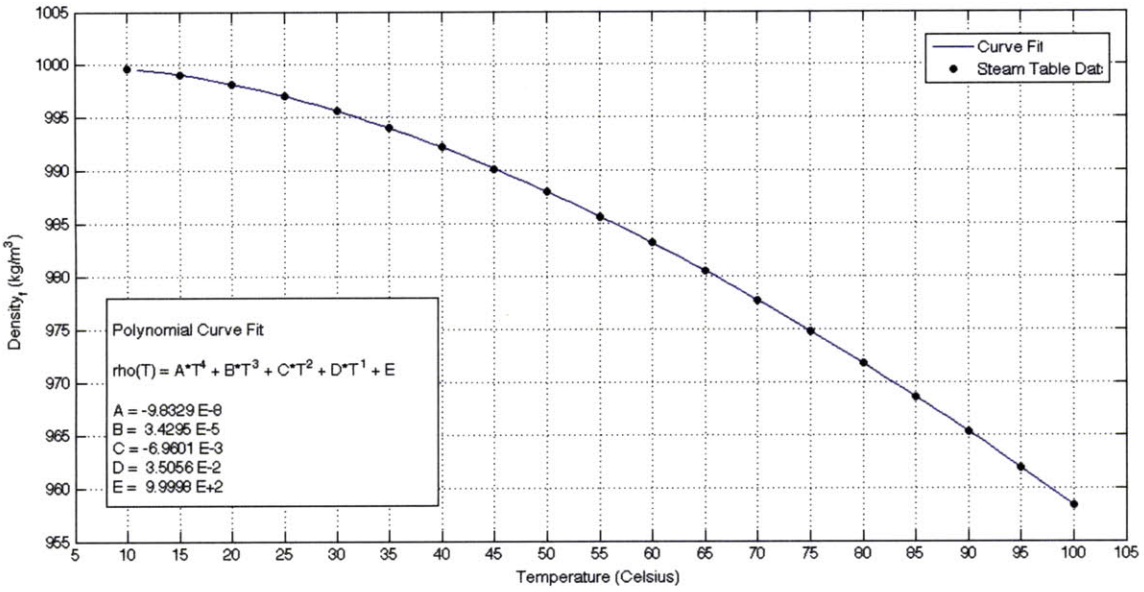

Water Viscosity (μ_f)

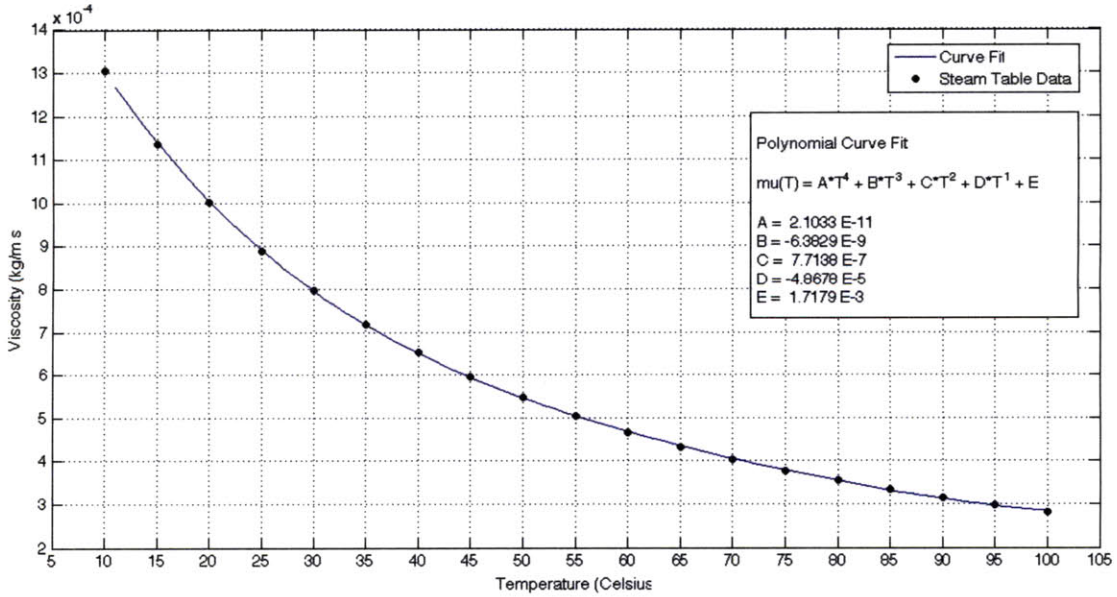

Water Thermal conductivity (k_f)

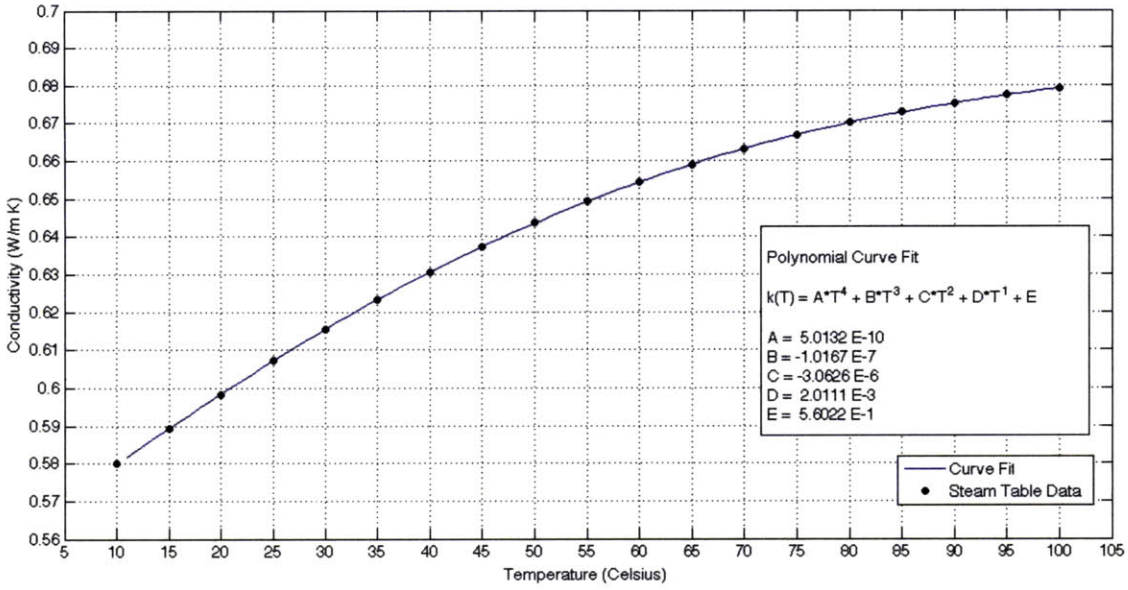

Water Prandtl number (Pr)

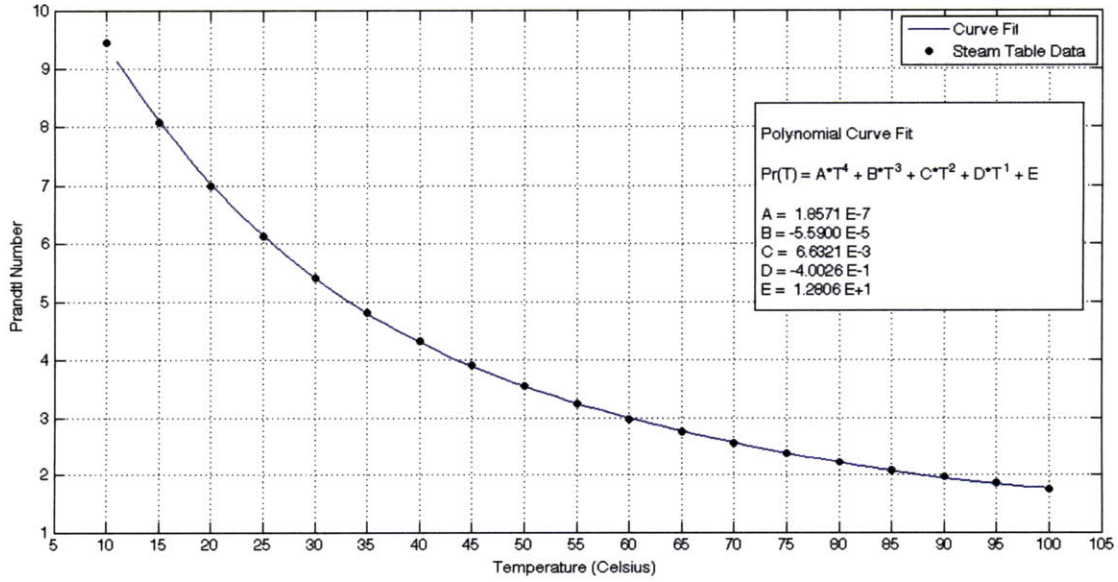

Section A.2. 180-second data average for water and silica nanofluid tests

	<TC1> (C)	<TC2> (C)	<TC3> (C)	<TC4> (C)	<TC5> (C)	<TC6> (C)	<TC7> (C)	<TC8> (C)	<TC9> (C)	<TC10> (C)	<TC0> (C)
Water 1	26.0410435	35.296441	40.5317888	44.6256149	46.7553975	50.6537081	52.8658012	55.5838882	57.9299565	59.2014162	60.0498385
Water 2	26.9895776	37.0294658	42.6783354	46.9341118	48.8678696	53.170236	55.4938882	58.4135093	60.5128137	61.9437578	62.716087
Water 3	28.4499506	39.6273333	45.9025803	50.390321	52.0638827	57.0702593	59.6879691	63.0096235	64.7130864	66.4699259	67.0034321
Water 4	28.8292531	41.2471914	48.1196482	52.9042222	54.4911358	60.034284	62.843784	66.4220803	67.9971667	69.9222161	70.2436235
Water 5	30.8974877	44.131858	51.4299321	56.3514259	57.7805679	63.6199753	66.618784	70.3878086	71.742642	73.8066852	74.0604198
SiO2 0.2 1	26.2206894	35.4190435	40.5721056	44.5400124	46.4551615	50.4655901	52.6216273	55.3485093	57.5204162	58.8423354	59.5148509
SiO2 0.2 2	28.6811111	40.0333765	46.268537	50.9417346	52.8494321	57.7166296	60.1436235	63.2117161	65.5176296	66.8408765	67.2494753
SiO2 0.2 3	29.1431296	41.2207222	47.9507531	52.5762654	54.0356914	59.4657161	62.2250803	65.8601543	67.2743148	69.1697099	69.4669877
SiO2 0.2 4	30.7219141	44.4773865	51.9069755	56.8144724	57.8953374	64.3036074	67.4006687	71.4375337	72.4293436	74.9349877	75.135865
SiO2 0.2 5	31.2784724	46.1206074	54.1089755	59.1938834	60.0029571	66.764546	69.8694908	74.2098712	74.6526012	77.6443374	77.3205828
SiO2 1% 1	26.0687037	35.5107407	40.7896914	44.8792593	47.102679	51.0255185	53.2515988	56.0682469	58.2325679	59.642537	60.4916975
SiO2 1% 2	28.5739136	40.417179	46.9890864	51.6144568	53.3247037	58.5180988	61.1990309	64.6617654	66.0732099	68.0770988	68.5455062
SiO2 1% 3	29.7291728	42.9796728	50.277463	55.2091173	56.8034753	62.654463	65.6132222	69.5160432	70.717537	72.9817099	73.2689198
SiO2 1% 4	31.0663395	45.9836358	53.9929321	59.2385062	60.5746852	67.1121543	70.3940309	74.694679	75.5301296	78.1715	78.3724383
SiO2 5% 1	25.0151914	34.0324198	39.1106543	43.1970309	45.5690803	49.3001914	51.5381667	54.3912284	56.5796482	58.1838951	59.1236728
SiO2 5% 2	24.8359938	34.4229815	39.7465	43.9793333	46.3631914	50.2878272	52.5739568	55.5562407	57.6498827	59.3460679	60.25
SiO2 5% 3	27.012537	37.6642778	43.5166358	48.0954444	50.5313765	54.8320309	57.3012469	60.4903086	62.6901914	64.3820494	65.2054136
SiO2 5% 4	27.1236914	38.1284568	44.1805062	48.8401728	51.1505926	55.6755185	58.1845617	61.4880803	63.4383457	65.2848272	65.9868272
SiO2 5% 5	28.5926235	41.0595062	47.8632901	52.820358	54.9119383	60.1680864	62.9564198	66.6719506	68.1830679	70.3910185	70.9872222

	<TIN> (C)	<Tout> (C)	<TestV> (VDC)	<SResV> (VDC)	<Flowrate> (HZ)	<Reynolds>	<Curr> (ADC)	<Power> (WAT)	<qflux>
Water 1	14.38817391	35.0435528	5.792372755	-0.0064351	205.8335357	777.5773479	-51.48079697	-298.1959656	-17137.69917
Water 2	14.89020497	35.04652174	6.167267475	-0.006837655	242.915748	917.6628213	-54.70124283	-337.3571956	-19388.34457
Water 3	15.61785802	35.54448148	6.703732293	-0.007408684	291.2757015	1100.352217	-59.26946963	-397.3266575	-22834.86537
Water 4	15.67938889	36.03778395	7.090247422	-0.007813673	320.379629	1210.298124	-62.50938252	-443.2069879	-25471.66597
Water 5	17.22481481	37.68489506	7.397029996	-0.00812903	347.860597	1314.112977	-65.03223862	-481.0454191	-27646.28845
SiO2 0.2 1	15.02985093	34.81215528	5.78212721	-0.00642346	223.2785796	843.47949	-51.38768159	-297.130112	-17076.44322
SiO2 0.2 2	16.2406358	37.00695679	6.594838188	-0.007281904	275.5949762	1041.115141	-58.25523477	-384.1838467	-22079.53142
SiO2 0.2 3	16.62674074	36.28512963	7.011394502	-0.007727702	317.7302865	1200.289703	-61.82161254	-433.4557142	-24911.24794
SiO2 0.2 4	17.0178589	37.21444785	7.668091993	-0.00841831	374.722432	1415.588931	-67.3464776	-516.4189856	-29679.25205
SiO2 0.2 5	16.88132515	36.71473006	8.064204285	-0.00883714	426.0751544	1609.584111	-70.69712088	-570.1160252	-32765.2888
SiO2 1% 1	14.3837716	34.44747531	5.927632475	-0.006582495	230.9330428	872.3957559	-52.65995926	-312.1488846	-17939.59107
SiO2 1% 2	15.6946358	35.02946914	6.969643608	-0.007691904	324.5419077	1226.021965	-61.53522958	-428.8786194	-24648.19652
SiO2 1% 3	16.03951852	36.03938272	7.496042385	-0.008244584	380.1734112	1436.181095	-65.9566759	-494.4140379	-28414.59988
SiO2 1% 4	16.70551852	37.09466049	8.043549679	-0.008811021	415.0033012	1567.757971	-70.48816583	-566.9750638	-32584.77378
SiO2 5% 1	13.63207407	33.94703086	5.823388988	-0.006474278	216.7268185	818.7289021	-51.79422119	-301.6178972	-17334.36191
SiO2 5% 2	13.11798765	33.05130864	6.089462057	-0.006765237	247.7261693	935.8351498	-54.12189965	-329.5732543	-18940.99163
SiO2 5% 3	14.99227778	35.86003086	6.4434292	-0.007129064	265.9683483	1004.748629	-57.03251565	-367.4849765	-21119.82624
SiO2 5% 4	14.66472222	34.8345	6.693198252	-0.007401477	295.1442369	1114.966384	-59.21181822	-396.316438	-22776.80678
SiO2 5% 5	15.29680864	35.14114815	7.328932526	-0.008073774	362.8547338	1370.756328	-64.59019017	-473.3771454	-27205.58307

Section A.3. MATLAB .m code for heat transfer analysis

```
clear;
Water=[
RAW DATA];

Si5=[
RAW DATA];

Si1=[
RAW DATA];

Si02=[
RAW DATA];


Di=0.218*0.0254;
Do=0.25*0.0254;
L=1;
mu24=0.000912684;
mdc=0.218*0.0254/4;

kp_s=1.38;
rho_p=2250;
cp_s=745;

Re=Water(:,17);
Q=-Water(:,19);
q=-Water(:,20);
Tin=Water(:,12);
Tout=Water(:,13);
DT=(Tout-Tin);

Re5=Si5(:,17);
Q5=-Si5(:,19);
q5=-Si5(:,20);
Tin5=Si5(:,12);
Tout5=Si5(:,13);
DT5=(Tout5-Tin5);
phi5=0.05;

Re1=Si1(:,17);
Q1=-Si1(:,19);
q1=-Si1(:,20);
Tin1=Si1(:,12);
Tout1=Si1(:,13);
DT1=(Tout1-Tin1);
phi1=0.01;

Re02=Si02(:,17);
Q02=-Si02(:,19);
q02=-Si02(:,20);
Tin02=Si02(:,12);
Tout02=Si02(:,13);
DT02=(Tout02-Tin02);
phi02=0.002;

%muSi02()=-1.5024e-5*Temp()+0.001262262;
%muSi1()=-1.7571e-5*Temp()+0.001503036;
%muSi5()=-2.0119e-5*Temp()+0.0017438;

for u=1:5
    muW(u)=2.1033e-11*Tin(u)^4-6.3829e-9*Tin(u)^3+7.7138e-7*Tin(u)^2-4.8678e-5*Tin(u)+0.0017179;
    rhoW(u)=-9.8329e-8*Tin(u)^4+3.4295e-5*Tin(u)^3-0.0069601*Tin(u)^2+0.035056*Tin(u)+999.9753;
    v(u)=Re(u)*muW(u)/(rhoW(u)*Di);

    rhoSiW5(u)=-9.8329e-8*Tin5(u)^4+3.4295e-5*Tin5(u)^3-
0.0069601*Tin5(u)^2+0.035056*Tin5(u)+999.9753;
    rhoSi5(u)=phi5*rho_p+(1-phi5)*rhoSiW5(u);
    muSi5(u)=-2.0119e-5*Tin5(u)+0.0017438;
    v5(u)=Re5(u)*muSi5(u)/(rhoSi5(u)*Di);
```

```
    rhoSiW02(u)=-9.8329e-8*Tin02(u)^4+3.4295e-5*Tin02(u)^3-
0.0069601*Tin02(u)^2+0.035056*Tin02(u)+999.9753;
    rhoSi02(u)=phi02*rho_p+(1-phi02)*rhoSiW02(u);
    muSi02(u)=-1.5024e-5*Tin02(u)+0.001262262;
    v02(u)=Re02(u)*muSi02(u)/(rhoSi02(u)*Di);
end

for uu=1:4
    rhoSiW1(uu)=-9.8329e-8*Tin1(uu)^4+3.4295e-5*Tin1(uu)^3-
0.0069601*Tin1(uu)^2+0.035056*Tin1(uu)+999.9753;
    rhoSi1(uu)=phi1*rho_p+(1-phi1)*rhoSiW1(uu);
    muSi1(uu)=-1.7571e-5*Tin1(uu)+0.001503036;
    v1(uu)=Re1(uu)*muSi1(uu)/(rhoSi1(uu)*Di);
end

for a=1:5
    for b=1:11
        x(b)=(b-1)/10;
        Le(a)=Di*0.06*Re(a);

        BTemp(a,b)=Tin(a)+(b-1)*DT(a)/10;

        kW(a,b)=0.0127*Water(a,b)+13.23188;
        Twi(a,b)=Water(a,b)-Q(a)/(2*pi*kW(a,b)*L)*((Do^2)/(Do^2-Di^2)*log(Do/Di)-0.5);

        Pr(a,b)=1.8571e-7*BTemp(a,b)^4-5.5900e-5*BTemp(a,b)^3+6.6321e-3*BTemp(a,b)^2-
0.40026*BTemp(a,b)+12.806;
        k(a,b)=5.0132e-10*BTemp(a,b)^4-1.0167e-7*BTemp(a,b)^3-3.0626e-
6*BTemp(a,b)^2+0.0020111*BTemp(a,b)+0.56022;
        rho(a,b)=-9.8329e-8*BTemp(a,b)^4+3.4295e-5*BTemp(a,b)^3-
0.0069601*BTemp(a,b)^2+0.035056*BTemp(a,b)+999.9753;
        mu(a,b)=2.1033e-11*BTemp(a,b)^4-6.3829e-9*BTemp(a,b)^3+7.7138e-7*BTemp(a,b)^2-4.8678e-
5*BTemp(a,b)+0.0017179;
        cp(a,b)=2.3140e-6*BTemp(a,b)^4-5.9167e-4*BTemp(a,b)^3+0.062170*BTemp(a,b)^2-
2.6184*BTemp(a,b)+4216.5;

        md(a)=pi*mu24*mdc*Re(a);
        fl(a)=md(a)*264.172*60/(rho(a,b));
        P(a)=md(a)*(cp(a,b)*Tout(a)-cp(a,b)*Tin(a));
        DP(a)=(Q(a)-P(a)')/(P(a)');

        Re(a,b)=v(a)*Di*rho(a,b)/mu(a,b);

        xp(a,b)=2*(x(b)/Di)/(Re(a,b)*Pr(a,b));

        qP(a)=P(a)/(pi*Di);
        hP(a,b)=qP(a)/(Twi(a,b)-BTemp(a,b));
        h(a,b)=q(a)/(Twi(a,b)-BTemp(a,b));
        Nu(a,b)=h(a,b)*Di/k(a,b);
        NuP(a,b)=hP(a,b)*Di/k(a,b);

        NuC(a,b)=4.933+0.1221*xp(a,b)^-0.6478*exp(-7.834*xp(a,b));
        NuL(a,b)=4.364+0.263*(xp(a,b)/2)^-0.506*exp(-20.5*xp(a,b));

        DNu(a,b)=NuP(a,b)/NuL(a,b);
        Le(a,b)=Di*0.06*Re(a,b);
    end
end

for y5=1:length(Re5)
    for z5=1:11
        Le5(y5)=Di*0.06*Re5(y5);

        BTemp5(y5,z5)=Tin5(y5)+(z5-1)*DT5(y5)/10;

        kB5(y5,z5)=0.0127*Si5(y5,z5)+13.23188;
        Twi5(y5,z5)=Si5(y5,z5)-Q5(y5)/(2*pi*kB5(y5,z5)*L)*((Do^2)/(Do^2-Di^2)*log(Do/Di)-0.5);

        kWSi5(y5,z5)=5.0132e-10*BTemp5(y5,z5)^4-1.0167e-7*BTemp5(y5,z5)^3-3.0626e-
6*BTemp5(y5,z5)^2+0.0020111*BTemp5(y5,z5)+0.56022;
        kSi5(y5,z5)=(1+3*(kp_s-kWSi5(y5,z5))*phi5/(kp_s+2*kWSi5(y5,z5)-(kp_s-
kWSi5(y5,z5))*phi5))*kWSi5(y5,z5);
        cpW5(y5,z5)=2.3140e-6*BTemp5(y5,z5)^4-5.9167e-4*BTemp5(y5,z5)^3+0.062170*BTemp5(y5,z5)^2-
```

```
2.6184*BTemp5(y5,z5)+4216.5;
        rhoW5(y5,z5)=-9.8329e-8*BTemp5(y5,z5)^4+3.4295e-5*BTemp5(y5,z5)^3-
0.0069601*BTemp5(y5,z5)^2+0.035056*BTemp5(y5,z5)+999.9753;

        rho5(y5,z5)=phi5*rho_p+(1-phi5)*rhoW5(y5,z5);
        cp5(y5,z5)=(phi5*rho_p*cp_s+(1-phi5)*rhoW5(y5,z5)*cpW5(y5,z5))/rho5(y5,z5);
        mu5(y5,z5)=-2.0119e-5*BTemp5(y5,z5)+0.0017438;
        Pr5(y5,z5)=mu5(y5,z5)*cp5(y5,z5)/kSi5(y5,z5);

        md5(y5)=pi*mu24*mdc*Re5(y5);
        fl5(y5)=md5(y5)*264.172*60/(rho5(y5,z5));
        P5(y5)=md5(y5)*(cp5(y5,z5)*Tout5(y5)-cp5(y5,z5)*Tin5(y5));
        DP5(y5)=(Q5(y5)-P5(y5)')/(P5(y5)');

        q5(y5)=P5(y5)/(pi*Di);
        h5(y5,z5)=q5(y5)/(Twi5(y5,z5)-BTemp5(y5,z5));
        Nu5(y5,z5)=h5(y5,z5)*Di/kSi5(y5,z5);

        Re5(y5,z5)=v5(y5)*Di*rho5(y5,z5)/mu5(y5,z5);
        xp5(y5,z5)=2*(x(z5)/Di)/(Re5(y5,z5)*Pr5(y5,z5));

        NuD5(y5,z5)=0.065*(1+0.0169*(phi5^0.15))*((Re5(y5,z5)^0.65)-60.22)*(Pr5(y5,z5)^0.542);
        NuC5(y5,z5)=4.649+0.1268*xp5(y5,z5)^-0.6113*exp(-21.43*xp5(y5,z5));
    end
end

for y1=1:length(Re1)
    for z1=1:11
        Le1(y1)=Di*0.06*Re1(y1);
        BTemp1(y1,z1)=Tin1(y1)+(z1-1)*DT1(y1)/10;

        kB1(y1,z1)=0.0127*Si1(y1,z1)+13.23188;
        Twi1(y1,z1)=Si1(y1,z1)-Q1(y1)/(2*pi*kB1(y1,z1)*L)*((Do^2)/(Do^2-Di^2)*log(Do/Di)-0.5);

        kWSi1(y1,z1)=5.0132e-10*BTemp1(y1,z1)^4-1.0167e-7*BTemp1(y1,z1)^3-3.0626e-
6*BTemp1(y1,z1)^2+0.0020111*BTemp1(y1,z1)+0.56022;
        kSi1(y1,z1)=(1+3*(kp_s-kWSi1(y1,z1))*phi1/(kp_s+2*kWSi1(y1,z1)-(kp_s-
kWSi1(y1,z1))*phi1))*kWSi1(y1,z1);
        cpW1(y1,z1)=2.3140e-6*BTemp1(y1,z1)^4-5.9167e-4*BTemp1(y1,z1)^3+0.062170*BTemp1(y1,z1)^2-
2.6184*BTemp1(y1,z1)+4216.5;
        rhoW1(y1,z1)=-9.8329e-8*BTemp1(y1,z1)^4+3.4295e-5*BTemp1(y1,z1)^3-
0.0069601*BTemp1(y1,z1)^2+0.035056*BTemp1(y1,z1)+999.9753;

        rho1(y1,z1)=phi1*rho_p+(1-phi1)*rhoW1(y1,z1);
        mu1(y1,z1)=-1.7571e-5*BTemp1(y1,z1)+0.001503036;
        cp1(y1,z1)=(phi1*rho_p*cp_s+(1-phi1)*rhoW1(y1,z1)*cpW1(y1,z1))/rho1(y1,z1);
        Pr1(y1,z1)=mu1(y1,z1)*cp1(y1,z1)/kSi1(y1,z1);

        md1(y1)=pi*mu24*mdc*Re1(y1);
        fl1(y1)=md1(y1)*264.172*60/(rho1(y1,z1));
        P1(y1)=md1(y1)*(cp1(y1,z1)*Tout1(y1)-cp1(y1,z1)*Tin1(y1));
        DP1(y1)=(Q1(y1)-P1(y1)')/(P1(y1)');

        q1(y1)=P1(y1)/(pi*Di);
        h1(y1,z1)=q1(y1)/(Twi1(y1,z1)-BTemp1(y1,z1));
        Nu1(y1,z1)=h1(y1,z1)*Di/kSi1(y1,z1);

        Re1(y1,z1)=v1(y1)*Di*rho1(y1,z1)/mu1(y1,z1);
        xp1(y1,z1)=2*(x(z1)/Di)/(Re1(y1,z1)*Pr1(y1,z1));

        NuD1(y1,z1)=0.065*(1+0.0169*(phi1^0.15))*((Re1(y1,z1)^0.65)-60.22)*(Pr1(y1,z1)^0.542);
        NuC1(y1,z1)=4.771+0.1810*xp1(y1,z1)^-0.5798*exp(-7.803*xp1(y1,z1));
    end
end

for y2=1:length(Re02)
    for z2=1:11
        Le2(y2)=Di*0.06*Re02(y2);
        BTemp02(y2,z2)=Tin02(y2)+(z2-1)*DT02(y2)/10;

        kB02(y2,z2)=0.0127*Si02(y2,z2)+13.23188;
        Twi02(y2,z2)=Si02(y2,z2)-Q02(y2)/(2*pi*kB02(y2,z2)*L)*((Do^2)/(Do^2-Di^2)*log(Do/Di)-
0.5);
```

```
        kWSi2(y2,z2)=5.0132e-10*BTemp02(y2,z2)^4-1.0167e-7*BTemp02(y2,z2)^3-3.0626e-
6*BTemp02(y2,z2)^2+0.0020111*BTemp02(y2,z2)+0.56022;
        kSi2(y2,z2)=(1+3*(kp_s-kWSi2(y2,z2))*phi02/(kp_s+2*kWSi2(y2,z2)-(kp_s-
kWSi2(y2,z2))*phi02))*kWSi2(y2,z2);
        cpW2(y2,z2)=2.3140e-6*BTemp02(y2,z2)^4-5.9167e-
4*BTemp02(y2,z2)^3+0.062170*BTemp02(y2,z2)^2-2.6184*BTemp02(y2,z2)+4216.5;
        rhoW2(y2,z2)=-9.8329e-8*BTemp02(y2,z2)^4+3.4295e-5*BTemp02(y2,z2)^3-
0.0069601*BTemp02(y2,z2)^2+0.035056*BTemp02(y2,z2)+999.9753;

        rho2(y2,z2)=phi02*rho_p+(1-phi02)*rhoW2(y2,z2);
        mu2(y2,z2)=-1.5024e-5*BTemp02(y2,z2)+0.001262262;
        cp2(y2,z2)=(phi02*rho_p*cp_s+(1-phi02)*rhoW2(y2,z2)*cpW2(y2,z2))/rho2(y2,z2);
        Pr2(y2,z2)=mu2(y2,z2)*cp2(y2,z2)/kSi2(y2,z2);

        md2(y2)=pi*mu24*mdc*Re02(y2);
        fl2(y2)=md2(y2)*264.172*60/(rho2(y2,z2));
        P2(y2)=md2(y2)*(cp2(y2,z2)*Tout02(y2)-cp2(y2,z2)*Tin02(y2));
        DP2(y2)=(Q02(y2)-P2(y2)')/(P2(y2)');

        q2(y2)=P2(y2)/(pi*Di);
        h2(y2,z2)=q2(y2)/(Twi02(y2,z2)-BTemp02(y2,z2));
        Nu2(y2,z2)=h2(y2,z2)*Di/kSi2(y2,z2);

        Re2(y2,z2)=v02(y2)*Di*rho2(y2,z2)/mu2(y2,z2);
        xp2(y2,z2)=2*(x(z2)/Di)/(Re2(y2,z2)*Pr2(y2,z2));

        NuD2(y2,z2)=0.065*(1+0.0169*(phi02^0.15))*((Re2(y2,z2)^0.65)-60.22)*(Pr2(y2,z2)^0.542);
        NuC2(y2,z2)=5.179+0.1728*xp2(y2,z2)^-0.5988*exp(-13.82*xp2(y2,z2));
        NuU2(y2,z2)=1.619*(xp(y2,z2)^(-1/3));
    end
end


clear plot;
hold off;

plot(xp2',Nu2','bo');
hold on;grid;

xlabel('x+');
ylabel('Nusselt Number  ');
plot(xp2',NuC2','b');
plot(xp2',NuU2','r');
%plot(xp1',NuC1','r');
%plot(xp5',Nu5','go');
%plot(xp5',NuC5','g');
%plot(xp',NuP','yo');
%plot(xp',NuC','y');
%plot(xp',NuL','c');
```

Section A.4. Heat transfer characteristics modeling

To compare the heat transfer characteristics and trends of the different silica nanofluid concentrations, curve fits are established close to the Nusselt number data points. A suitable fit type that can be compared in detail is in the format of Eq. (17). Table 5.2 shows the coefficients of the curve fits from all nanofluid experiments as well as the deionized water test.

ϕ	A	B	C	n
0.05	4.649	0.1268	21.43	-0.6113
0.01	4.771	0.1810	7.803	-0.5798
0.002	5.179	0.1728	13.82	-0.5988
0 (Water)	4.933	0.1221	7.834	-0.6478
Lienhard	4.364	0.263	20.5	-0.506
$Nu(x_+) = A + B\cdot(x_+)^n\cdot\exp(-C\cdot x_+)$				

Coefficient **A** illustrates that the relative intercept of the curve, or offset. Higher values of this coefficient show that heat transfer coefficients are generally higher on the entire curve. Thus, it is observed that with increasing concentration of silica nanofluid, the heat transfer coefficient decreases.

Coefficient **B** reflects the rate of the curve, or slope. Higher values means that physically, the heat transfer coefficients decrease faster through developing flows. Coefficient **C** is the rate attributed to the exponential curve. The factor **n** is the exponential in the power function of the dimensionless distance, or Graetz number. The absolute higher **n** causes the power function to decay at a faster rate.

BIBLIOGRAPHY

[1] M.J. Assael, E. Charitidou, S. Avgoustiniatos, and W.A. Wakeham. Absolute Measurements of the Thermal Conductivity of Mixtures of Alkene-Glycols with Water. *International Journal of Thermophysics,* Volume 10, No. 6, 1989.

[2] J. Buongiorno, et. al. A Benchmark Study on the Thermal Conductivity of Nanofluids. *Journal of Applied Physics,* **106**, 094312, 2009.

[3] J.G. Brisson, E.G. Cravalho, G.H. McKinley, and J.L. Smith. *Thermal-Fluids Engineering II*. Oxford University Press, Cambridge, MA, 2009.

[4] CERAM Research, Ltd. *Silica-Silicon Dioxide*. Viewed March 19, 2010, Edited Dec. 13, 2001. http://www.azom.com/details.asp?articleid=1114.

[5] G.O. Curme and Franklin Johnston. *Glycols.* Reinhold Publishing Corp. New York, 1952.

[6] D.K. Das, R.S. Vajjha, and D.P. Kulkarni. Development of New Correlations for Convective Heat Transfer and Friction Factor in Turbulent Regime for Nanofluids. *International Journal of Heat and Mass Transfer*, 2010.

[7] Decagon Devices, Inc. *KD2 Pro Thermal Properties Analyzer, Operator's Manual.* Version 7, 2008-2009.

[8] Y. Ding, et. al. Heat Transfer Intensification Using Nanofluids. *KONA,* No. 25, 2007.

[9] J.G. Collier and J.R. Thome. *Convective Boiling and Condensation*, pp. 170 Fig. 4.21, Oxford University Press, 1999.

[10] A.H. Harvey, A.P. Peskin, and S.A. Klein. Thermodynamic Properties of H_2O (Liquid-Vapor Equilibrium). *NIST Standard Reference Data 10, NIST/ASME Steam Properties*, Version 2.1, 1997.

[11] J.H. Lienhard IV and J.H. Lienhard V. *A Heat Transfer Textbook*. Phlogiston Press Cambridge, MA. 2008.

[12] McMaster-Carr, Co. Gear, Rotary, and Piston Pumps. *McMaster-Carr Catalog*, pp. 331, 2010.

[13] A.F. Mills. *Basic Heat and Mass Transfer*. Prentice Hall. New Jersey. Table 4.10.

[14] OMEGA Technologies Co. *PX154 Series Pressure Transducer*, October 1994.

[15] OMEGA Technologies Co. Type K Reference Tables N.I.S.T. Monograph 175 Revised to ITS-90. *Revised Thermocouple References Tables*, pp. Z-204-Z-205, 1999.

[16] U. Rea. Experimental Study of Alumina-Water and Zirconia-Water Nanofluid Convective Heat Transfer and Viscous Pressure Loss in Laminar Regime. *Department of Mechanical Engineering at Massachusetts Institute of Technology*, February 2008.

[17] U. Rea, T. McKrell, L. Hu, and J. Buongiorno. Laminar Convective Heat Transfer and Viscous Pressure Loss of Alumina-Water and Zirconia-Water Nanofluids. *International Journal of Heat and Mass Transfer,* Volume 52, Issues 7-8, March 2009.

[18] R.K. Shah and A.L. London. *Laminar Flow Force Convection in Ducts,* pp. 40-42. Academic Press, New York, 1978.

[19] W.C. Williams. Experimental and Theoretical Investigation of Transport Phenomena in Nanoparticle Colloids (Nanofluids). *Department of Nuclear Science and Engineering at Massachusetts Institute of Technology*, December 2006.